COO-3246-16

RESEARCH IN NUCLEAR CHEMISTRY

Annual Progress Report
For Period September 15, 1975 - December 31, 1976

Morton Kaplan
Principal Investigator

Department of Chemistry
Carnegie-Mellon University
Pittsburgh, Pennsylvania 15213

October 1976

PREPARED FOR THE
U. S. ENERGY RESEARCH AND DEVELOPMENT ADMINISTRATION
UNDER CONTRACT NO. EY-76-S-02-3246

DISCLAIMER

COO-3246-16

RESEARCH IN NUCLEAR CHEMISTRY

CONTRACT EY-76-S-02-3246

ABSTRACT

We report the results of experimental studies in which the perturbations of gamma-ray angular correlations have been used to observe and measure the interactions of nuclear moments with chemically generated electric field gradients. Such quadrupole interactions can provide detailed information on molecular structure and chemical bonding. Experiments have been completed with ^{181}Hf binding to Vitamin B_{12} and ^{181}Hf and ^{111}Ag probes in DNA, as well as ^{181}Hf studies of several inorganic compounds containing Hf-oxygen and Hf-phosphate bonds. Experimental research programs in heavy-ion nuclear reactions studies have been initiated at several major accelerator facilities. At the ORNL Isochronous Cyclotron we are investigating the energetic fragments from heavy-ion transfer reactions on medium mass targets, using a counter telescope with element and mass resolution. Some results from ^{65}CU + ^{12}C at 130 MeV are presented. The emissions of H and He in hard grazing collisions of ^{86}Kr with ^{197}Au are being measured at the SuperHILAC accelerator of LBL. In this experiment, both singles measurements of the light charged particles and coincidence observations with deep inelastic processes are in progress. In a related, but distinct, experiment at the LBL 88" Cyclotron, we are studying the fusion, fission, and charged particle emission probabilities for ^{194}Hg compound nuclei excited to 97.5 MeV by different reactions using matched heavy-ion beams.

Morton Kaplan
Principal Investigator

TABLE OF CONTENTS

Contract EY-76-S-02-3246

(U. S. Energy Research and Development Administration---Carnegie-Mellon University)

Annual Report: October, 1976

I. Introduction

The nuclear science research program sponsored by Contract EY-76-S-02-3246 has undergone a significant reorientation in the past year. Our development and application of gamma-ray angular correlation techniques in hyperfine interactions studies has been very successful over the last few years, culminating in an intensive investigation of quadrupole perturbations which reflect the electric field gradients generated by chemical bonding. These experiments have now been effectively completed, and the results will be presented and discussed in this report. At the same time, we have expanded and refocussed our efforts in experimental heavy-ion nuclear reactions studies, and have established a firm foundation for on-going programs at several major accelerator facilities. These latter experiments are based upon the User Group concept, and we shall describe some of our work of the past year carried out at the Lawrence Berkeley Laboratory and Oak Ridge National Laboratory.

The objective of the perturbed-angular-correlation experiments was to determine the utility of nuclear quadrupole moments as sensitive microscopic probes of electron density distributions and dynamical motions in complex molecular systems. Using ^{181}Hf as the β-decay parent of a ^{181}Ta nuclear probe, we studied the nuclear quadrupole interactions in several inorganic insulators containing metal-oxygen and metal-phosphate bonds, in order to develop a familiarity with anticipated interactions in compounds of known structure and configuration. The results of these studies demonstrated the great sensitivity of the technique to detail, and we proceeded to extend the experiments to macromolecular species, among them Vitamin B_{12} (cyanocobalamin) and DNA, employing ^{181}Hf and ^{111}Ag as nuclear probes. The background material, experimental apparatus, and theoretical development have been presented in previous Annual Reports, particularly

COO-3246-15 (dated July, 1975), and we concentrate in Section II below on a summary of the experiments completed this year along with an interpretation of the data. This work has been presented in its entirety as the Ph.D. dissertation of E. J. Wilson, Carnegie-Mellon University, June 1976.

At the Oak Ridge National Laboratory we have been carrying out an experimental study of direct multinucleon processes in the interaction of energetic heavy ions with medium mass elements. In a long-term collaboration between Carnegie-Mellon University and Dr. Robert L. Ferguson of ORNL, we have bombarded thin ^{65}Cu targets with 130-MeV ^{12}C ions from the ORIC and analyzed the outgoing reaction products from Li through O by means of a ΔE-E counter telescope and multiparameter data acquisition system. The semiconductor-detector telescope arrangement was designed to yield resolution of adjacent masses as well as nuclear charges, and the data obtained in several runs has successfully demonstrated the attainment of this capability. A preliminary analysis of some of the experimental data will be presented in Section III of this report.

We have joined with Professor J. M. Miller of Columbia University and Professor J. M. Alexander of SUNY, Stony Brook, to form a User Group at the Super-HILAC accelerator of the Lawrence Berkeley Laboratory. Our common interest is in the investigation of light charged particles emitted in hard grazing collisions of very heavy ions. During this past year, we have studied the energy and angular distributions of protons, deuterons, tritons, and alpha particles from the reactions of ^{197}Au with ^{86}Kr at 725 MeV. These results will be of particular importance in the interpretation of deep inelastic processes observed with high cross-sections for very heavy ions like Kr on heavy target nuclei. Very recently a more complex 8-parameter coincidence experiment was successfully carried out on the $^{86}Kr + ^{197}Au$ system at the SuperHILAC. In this work, a heavy fragment (either Kr or Au) from a deep inelastic event was detected at the appropriate angle in a

gas telescope, and the time-correlated protons and alpha particles were measured with a semi-conductor telescope system. From the energy and angular dependence of these measurements, we hope to be able to distinguish the charged particles which are emitted from separated Kr-like and Au-like fragments as well as those which originate from "hot necks" before the fragments separate.

The Columbia, Stony Brook, Carnegie-Mellon team are also performing measurements of fusion, fission, and charged-particle emission cross-sections for selected compound nucleus reactions. These experiments, carried out at the 88" Cyclotron of the Lawrence Berkeley Laboratory, involve the formation of ^{194}Hg compound nuclei in two different ways at the same excitation energy but with differing angular momentum distributions in the entrance channels. The systems chosen are ^{182}W + ^{12}C at 121 MeV and ^{175}Lu + ^{19}F at 135 MeV to yield ^{194}Hg at an excitation of 100 MeV. As ^{194}Hg is an approximation to ^{197}Au, the importance and relationship of these studies to the ^{86}Kr + ^{197}Au experiments at the SuperHILAC becomes evident when one recognizes the significance of different contributing partial-waves to competing nuclear reaction mechanisms.

Finally, a preliminary experiment has been run at the SuperHILAC, in which recoil techniques and radioactivity counting are used to compare excitation functions for Ar and Ne induced reactions.

During the past contract period, the experimental researches carried out at Carnegie-Mellon University made use of the facilities and equipment of our laboratory as described in previous annual reports. No major changes in instrumentation or nuclear counting equipment have been made this year, and minor improvements may be mentioned where relevant elsewhere in this report. For the experiments at ORNL and LBL, detectors and detector systems have been purchased and fabricated, with the necessary counting electronics being derived mostly from the Users' Pools supplemented by some of our own units. In June of this year, we were the first

group to use the new 30" scattering chamber at the SuperHILAC and we hope our experiences have contributed to the continuing improvement of the system. In October we were also first in employing the new Mod Comp IV computer as a primary data acquisition device and its outstanding capabilities and performance were instrumental in the success of our experiment. This past year the principal investigator, Professor Morton Kaplan, devoted one-half time to the research project during the academic year and full time for two summer months. Jane Wilson, Project Scientist, has completed her Ph.D. dissertation research in the program supported by the contract, and has written her thesis on the angular correlation experiments. Professor A. A. Caretto and Drs. J. C. Love and J. W. Ball have participated in various aspects of the heavy-ion reactions studies. As in the past, we have benefited from the strong interactions among the nuclear scientists at Carnegie-Mellon University.

In the following pages, we shall describe in greater detail the experimental programs and research progress outlined above. A number of scientific papers based on the contract-supported research are being prepared for publication, and a current listing is appended to this report.

II. Perturbed Angular Correlations of Nuclear Gamma Rays

A. Nuclear Quadrupole Interactions in Simple Hafnium Inorganic Compounds

During the past year, we have completed a study by the time-differential perturbed angular correlation (TDPAC) technique of the nuclear quadrupole interactions of ^{181}Ta in simple hafnium compounds containing oxygen-hafnium bonds. Certain aspects of this research, including details of experimental set-up and data-analysis procedures, have been previously reported in COO-3246-15 (Annual Report, July 1975). The extensive and updated experimental results will be presented here.

The experiments were performed using the 42.5 d isotope, ^{181}Hf, which β^- decays predominantly to the 615 keV (I = 1/2+) state in ^{181}Ta, as indicated in the decay scheme[1] in Fig. 1. The decay to the tantalum ground state is mainly through two gamma-ray cascades, the 133-482 keV cascade being of importance to this work. The long half-life (10.8 nsec) of the intermediate 5/2+ state, coupled with its large nuclear quadrupole moment ($\sim 2.5 \times 10^{-24}$ cm^2) makes it an ideal probe for the study of chemically generated electric quadrupole interactions.

A fairly extensive description of the theoretical treatment of the nuclear quadrupole interaction in polycrystalline solids and in solutions of macromolecular species was given earlier in COO-3246-15. Therefore, only a brief enunciation of the major equations and terms describing the physical situation will be given. The coupling of the nuclear quadrupole moment, Q, of the intermediate nuclear state with spin I = 5/2 in a gamma-gamma nuclear cascade with a static electric field gradient (EFG), $V_{zz} = \partial^2 V/\partial z^2$, generated by the electronic distribution surrounding the nucleus is described by the following.[2]

$$G_{kk}(t) = S_{ko} + \sum_{n=1}^{3} S_{kn} \exp(-1/2\ \delta^2 \omega_n^2 t^2) \cos(\omega_n t) \qquad (1)$$

Figure 1.

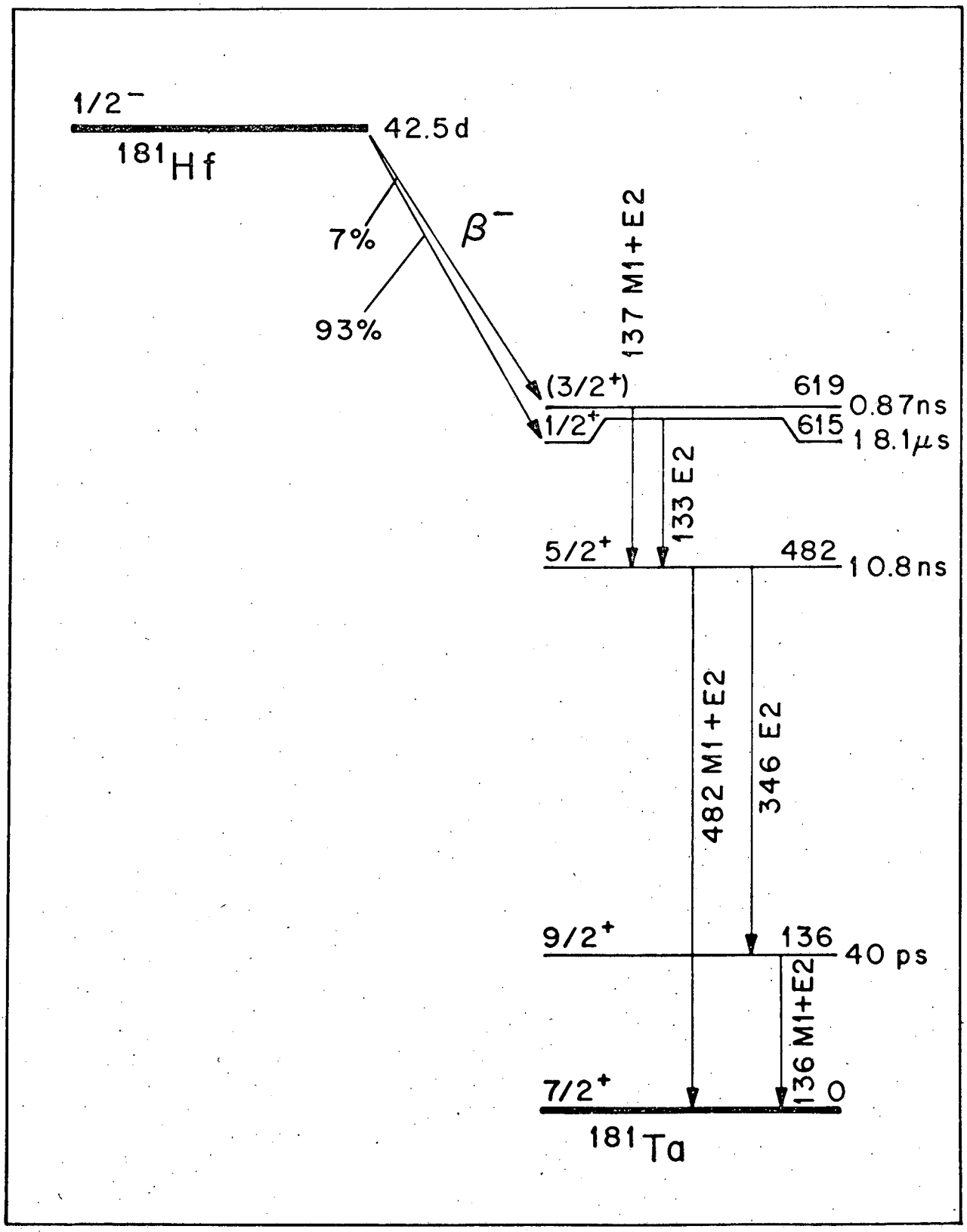
1/2⁻
181Hf
42.5d
7%
93%
β⁻
137 M1+E2
(3/2⁺)
619
0.87ns
1/2⁺
615
18.1μs
133 E2
5/2⁺
482
10.8ns
482 M1+E2
346 E2
9/2⁺
136
40 ps
136 M1+E2
7/2⁺
0
181Ta

The perturbation coefficient, $G_{kk}(t)$, depends upon an interaction frequency, ω_n, which for a randomly oriented static axially symmetric ($\eta = 0$) EFG corresponds to the smallest nonvanishing energy difference between the nuclear m states split by the interaction. If the asymmetry parameter, $\eta = 0$, $\omega_1 \equiv \omega_o = 6\ \omega q$ where the quadrupole frequency is defined by

$$\omega_q = \frac{eQ\ V_{zz}}{4I(I-1)\hbar} \tag{2}$$

The remaining two frequencies in equation (1) are harmonics of ω_o. The electric field gradient components and asymmetry parameter are related in the standard way:

$$\eta = \frac{V_{xx} - V_{yy}}{V_{zz}}$$

$$|V_{zz}| \geq |V_{yy}| \geq |V_{xx}| \tag{3}$$

$$V_{zz} + V_{yy} + V_{xx} = 1$$

$$0 \leq \eta \leq 1$$

For a rhombic EFG (i.e., $\eta \neq 0$), the harmonicity of the interaction frequencies is lost and ω_1 is no longer simply related to ω_q. Reference to Figure 2 gives the relationship of ω_1 to ω_q as η increases.[3] The exponential term in equation (1) accounts for any source inhomogeneities which give rise to a small distribution in frequencies about the mean, ω_n. It is characterized by a distribution parameter or spread, δ. For all work presented here, terms with $k > 4$ were considered negligible. The values of the coefficients in equation (1) reflect the source type, geometry and spatial orientation (i.e., single crystal coefficients are quite different from those to be expected from a polycrystalline source).

The top spectrum in Fig. 3 gives the results for ^{181}Hf dissolved in 27 N

Figure 2.

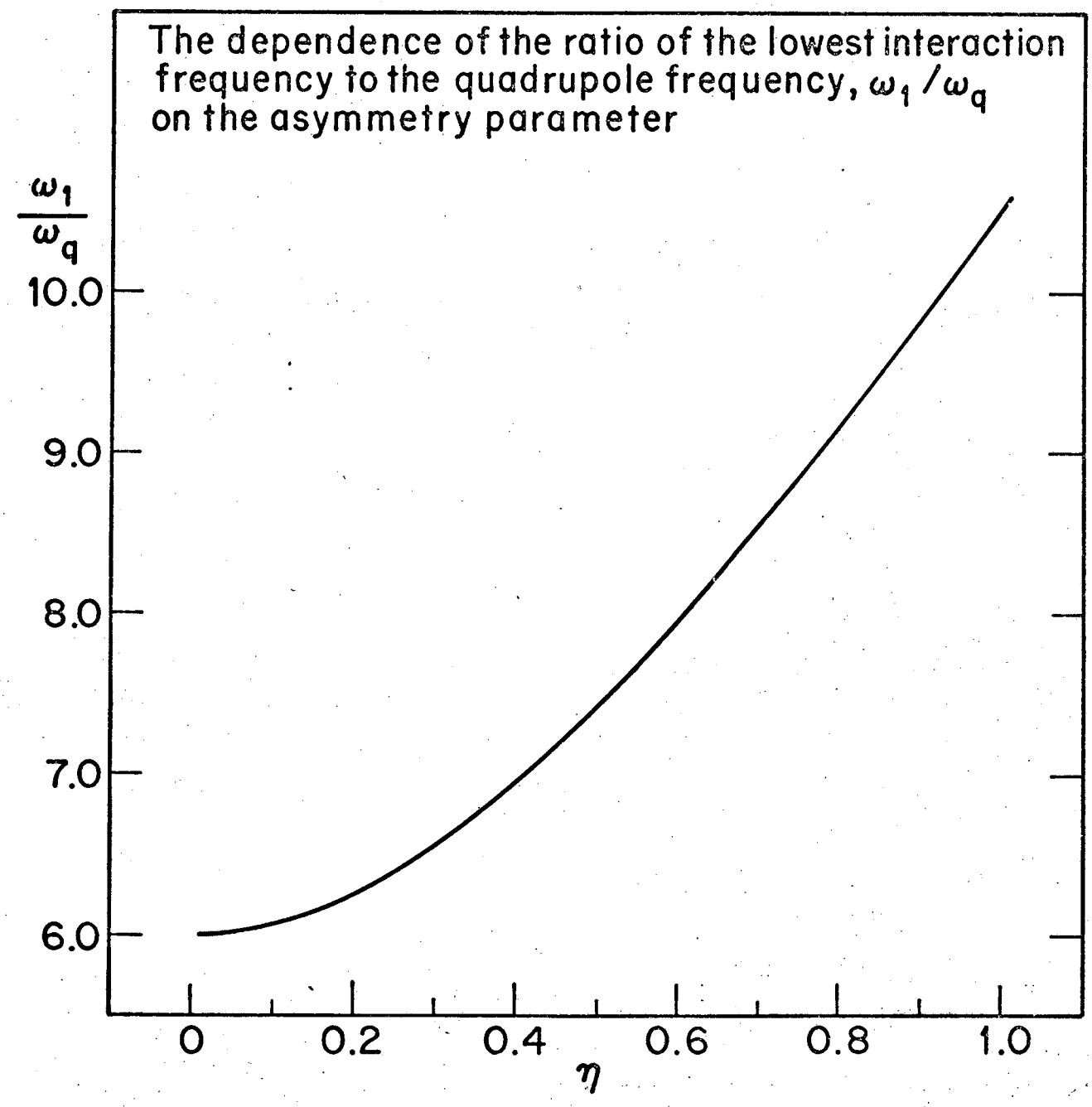
The dependence of the ratio of the lowest interaction frequency to the quadrupole frequency, ω_1/ω_q on the asymmetry parameter
$\frac{\omega_1}{\omega_q}$
10.0
9.0
8.0
7.0
6.0
0
0.2
0.4
0.6
0.8
1.0
η

HF, forming the $[HfF_6]^{-2}$ complex. As would be expected for an octahedral complex, no perturbation of the intermediate nuclear state occurs. The product of the angular correlation coefficient and the perturbation coefficient, $A_{22}G_{22}(t)$ vs. time is a flat line with an average value equal to the angular correlation coefficient (i.e., $G_{22}(t) = 1.0$). The resulting value for A_{22} after correction for the solid angles of the detectors and any system non-linearities is $A_{22} = -0.295 \pm 0.005$. This is in excellent agreement with the adopted value of $A_{22} = -0.295 \pm 0.010$[4], and confirms that our system is free of extraneous perturbations. The initial rise in the data results from the attenuating effect of the finite resolving time of the experimental apparatus.

The oxide of hafnium is monoclinic, with four HfO_2 units forming a face centered monoclinic crystal with a hafnium nucleus at each corner and face. Each hafnium nucleus is surrounded by eight oxygens nearest neighbors and may be bound to all eight simultaneously.[5] The sample preparation procedures, least squares fitting and major results were presented in detail in COO-3246-15. However, the interaction frequency, ω_1, previously reported there was not corrected for the nonaxial symmetry of the EFG and a higher apparent ω_q resulted. The second spectrum from the top in Fig. 3 presents the data plus fit to our HfO_2 sample. The resulting corrected value for the quadrupole frequency, ω_q, along with those for the asymmetry parameter and the spread in frequencies due to source inhomogeneities, δ, are

$$\omega_q = 122.8 \pm 6.6 \text{ MH}_z$$
$$\eta = 0.43 \pm 0.08$$
$$\delta = 0.04 \pm 0.01$$

Our value of ω_q and η, coupled with the quadrupole moment of the intermediate nuclear state ($Q(5/2) = 2.5 \times 10^{-24}$ cm^2) result in the following values for the electric field gradient components

Figure 3.

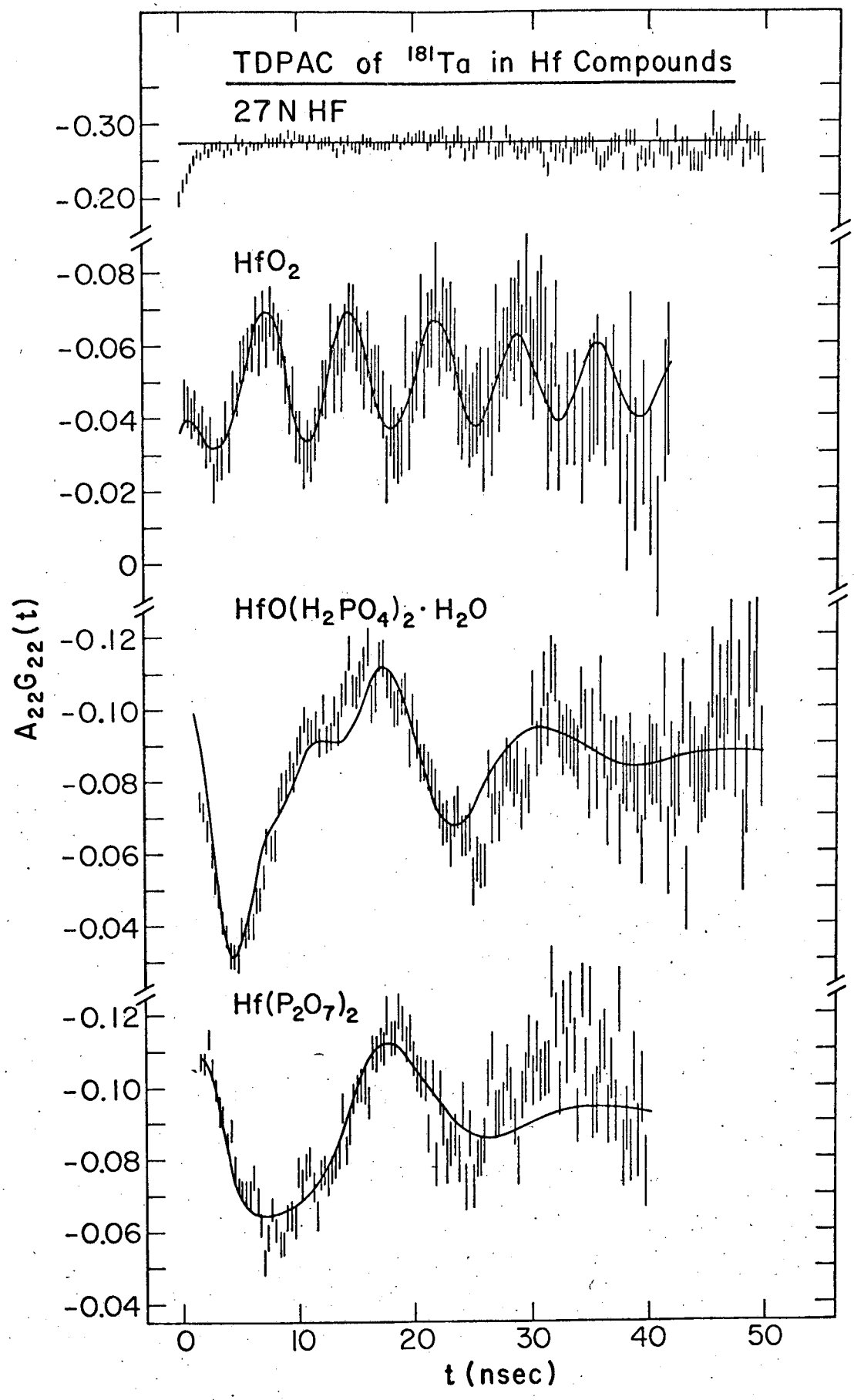
TDPAC of ^{181}Ta in Hf Compounds
27 N HF
HfO_2
$HfO(H_2PO_4)_2 \cdot H_2O$
$Hf(P_2O_7)_2$
$A_{22}G_{22}(t)$
t (nsec)
-0.30
-0.20
-0.08
-0.06
-0.04
-0.02
0
-0.12
-0.10
-0.08
-0.06
-0.04
-0.12
-0.10
-0.08
-0.06
-0.04
0
10
20
30
40
50

$$|V_{zz}| = (1.28 \pm 0.07) \times 10^{18} \text{ V/cm}^2$$
$$|V_{yy}| = (0.916 \pm 0.178) \times 10^{18} \text{ V/cm}^2$$
$$|V_{xx}| = (0.365 \pm 0.071) \times 10^{18} \text{ V/cm}^2$$

Our value of the quadrupole frequency compares quite well with previous experiments on HfO_2.[3,6,7]

Hafnium forms a disubstituted phosphate which exhibits the structure below

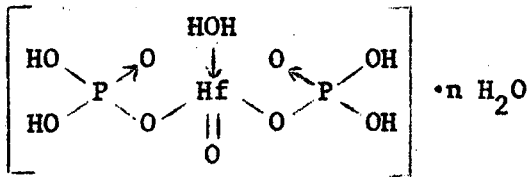

In order to minimize the influence of δ, the hafnium phosphate was prepared by homogeneous precipitation from metaphosphoric acid solution. Details of the procedure are available in reference 8.

The TDPAC data and best fit curve (solid line) are given in the third spectrum in Fig. 3. The resulting values for the interaction frequencies and δ are

$$\omega_1 = 399 \pm 6 \text{ MHz}$$
$$\omega_2 = 678 \pm 26 \text{ MHz}$$
$$\eta = 0.38 \pm 0.05$$
$$\delta = 0.18 \pm 0.01$$

The frequencies, ω_n, lead to a quadrupole frequency of $\omega_q = 58 \pm 2$ MHz, for an asymmetry parameter of $\eta = 0.38 \pm 0.05$. Using this value of η and ω_q, one obtains the following for the electric field gradient components

$$|V_{zz}| = (6.04 \pm 0.21) \times 10^{17} \text{ V/cm}^2$$
$$|V_{yy}| = (4.17 \pm 0.57) \times 10^{17} \text{ V/cm}^2$$
$$|V_{xx}| = (1.87 \pm 0.26) \times 10^{17} \text{ V/cm}^2$$

The magnitude and asymmetry of the EFG at the hafnium nucleus in the phosphate compound are comparable to quadrupole fields seen in many hafnium insulator and metallic compounds.[9-12] The persistance of the very large distribution in frequencies is attributable to a spreading effect of the varied number of waters of hydration about the hafnium. One water is always associated with the phosphate but any number (i.e., 5-7) may also be semibound. Their varied proximities or distances from the hafnium nucleus could create distortions of the EFG about the mean value of ω_n.

The final compound studied in this series was the pyrophosphate of hafnium, the structure of which is given below.

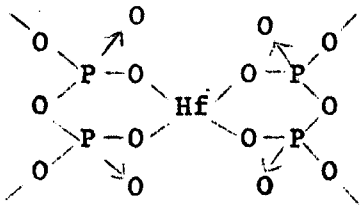

Hafnium is bound to four oxygens through sigma bonds arranged in a nearly cubic structure. A phosphate sample prepared by homogeneous precipitation from metaphosphoric acid solution was ignited at 1100°C to form the pyrophosphate compound. In order to reduce δ, the pyrophosphate was annealed 8 hours after completion of ignition.

The bottom spectrum in Fig. 3 gives the fit curve plus data. Even with the annealing procedure the sample exhibited a large δ which wiped out the fine structure within the first minimum and significantly damped the amplitude of later oscillations. The resulting parameters are:

$$\omega_1 = 346 \pm 5 \text{ MHz}$$

$$\omega_2 = 693 \pm 31 \text{ MHz}$$

$$\eta = 0.0 \pm 0.2$$

$$\delta = 0.185 \pm 0.015$$

The quadrupole frequency corresponding to an $\eta = 0.0 \pm 0.2$ is $\omega_q = 57.8 \pm 0.9$ MHz. Assuming $\eta = 0$, the EFG components, considering the error in ω_q only, are

$$|V_{zz}| = (6.00 \pm 0.09) \times 10^{17} \text{ V/cm}^2$$
$$|V_{yy}| = |V_{xx}| = |V_{zz}|/2 = (3.00 \pm 0.05) \times 10^{17} \text{ V/cm}^2$$

Both phosphate species exhibit quite similar quadrupole frequency magnitudes, but differ greatly in the magnitude of the asymmetry parameter. The large value of δ for the pyrophosphate is not easily attributable to waters of hydration and lacks a physically plausible explanation.

The experimental results for HfO_2 and the phosphates are summarized in Table I.

Table I. Compilation of the Major Numerical Results for Simple Polycrystalline Hf Compounds

Sample	ω_q (MHz)	η	Electric Field Gradient Components (10^{17} V/cm^2)		
			$\lvert V_{zz}\rvert$	$\lvert V_{yy}\rvert$	$\lvert V_{xx}\rvert$
$HfO(H_2PO_4)_2$	58.2 ± 2	0.38 ± 0.05	6.04 ± 0.21	4.17 ± 0.57	1.87 ± 0.26
HfO_2	122.8 ± 6.6	0.43 ± 0.08	12.8 ± 0.7	9.16 ± 1.78	3.65 ± 0.71
$Hf(P_2O_7)_2$	57.8 ± 0.9	0.0 ± 0.2	6.00 ± 0.09	3.00 ± 0.05	3.00 ± 0.05

The initial conclusion to be drawn from this work is that the nuclear quadrupole interaction of ^{181}Ta in hafnium compounds is a sensitive tool for the study of chemically generated electric field gradients. It was revealed that seemingly different hafnium structures lead to nearly the same magnitude of the EFG. The major change between the phosphate and pyrophosphate structures was the asymmetry parameter value. The much larger EFG for the oxide can be directly attributed to the greater number of bound oxygens at each hafnium. Considering the full valence bonding in the oxide, as well as the well-defined crystal structure, the much smaller δ value was to be expected. The study of the two

phosphate compounds, in which there was not a saturation of the hafnium valence orbitals and the consequent likelihood of bonding through waters of hydration, revealed that large frequency distributions will be characteristic of many hafnium compounds.

B. Nuclear Quadrupole Interactions in Macromolecular Species

1. Introduction

The study of the rotational correlation times, conformational changes and chemical structure of specific binding sites in macromolecular species should be amenable to the perturbed angular correlation technique. The sensitivity of the method to trace amounts of labels and the ability to study both the solid and liquid states allows the possibility of "in vivo" experimentation. In addition, the PAC method focuses on specific localized binding sites and is free of extraneous information originating from the solvent or the bulk of the macromolecules. Finally, the rigorous nature of the PAC theory allows the extraction of information unambiguously. Despite the obvious potential of the method, very few studies have, to date, been performed.[13-18] It was with the intention of exploring and further developing the method that a study of the nuclear quadrupole interactions of several macromolecular species was undertaken.

In addition to ^{181}Hf, the 7.5 d isotope ^{111}Ag was used for certain TDPAC studies on the macromolecular species. ^{111}Ag was obtained from Amersham-Searle Corporation as $[AgCl_4]^{-3}$ in 4 M HCl (carrier-free). It was converted to Ag_2O and then $AgNO_3$ according to the procedure given in reference 19. The resulting $^{111}AgNO_3$ stock solution was slightly acidic. A schematic level scheme giving the major decay features of the β^- emission of ^{111}Ag to ^{111}Cd is given in Fig. 4. Only a 6% component of the negatron decay feeds the 3/2+ state at 340 keV, with only an approximate 3% component passing through the 95-247 keV nuclear cascade of interest to this work. The 5/2+ state at 247 keV exhibits a radiative half life of 84 nsec and a quadrupole moment of $Q(5/2+) \simeq (0.60 \pm 0.11) \times 10^{-24}$

Figure 4.

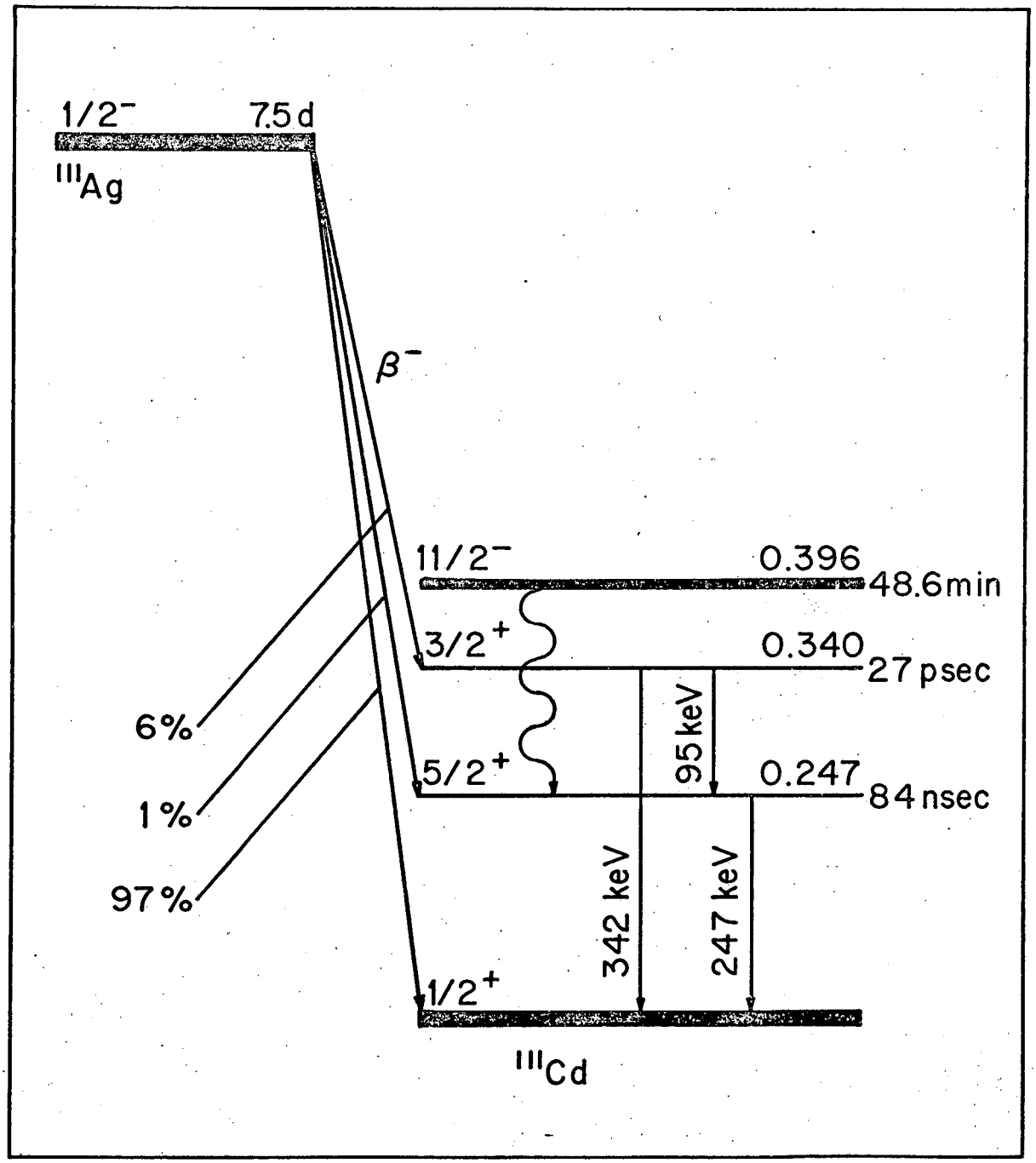
1/2⁻
7.5 d
111Ag
β⁻
11/2⁻
0.396
48.6 min
3/2⁺
0.340
27 psec
95 keV
6%
5/2⁺
0.247
84 nsec
1%
342 keV
247 keV
97%
1/2⁺
111Cd

cm^2. Due to the wide disparity of the reported measurements of Q[20-22], the figure quoted above is an average value with a fairly large error which will significantly increase the error in our reported electric field gradient components. The decay (wiggly line) of the often used 48.6 min state at 396 keV in ^{111m}Cd has been included for reference purposes only and is not populated in the ^{111}Ag decay.

Despite the low intensity of the ^{111}Ag gamma rays, their few number and energy separations should allow accurate setting of windows. Unfortunately, the only commercial supply (Amersham-Searle Corp.) of the parent ^{111}Ag contained an ~0.1% contamination of 253 d isotope ^{110m}Ag. The contamination results in a large and unresolved energy peak under the 95 keV gamma ray, which increases in relative magnitude as the ^{111}Ag decays. The influence of the contamination on the TDPAC data was carefully considered and corrected for. Detailed descriptions of the correction techniques may be found in reference 23. It should also be noted that the contamination contributed significantly (> 50%) to the source gamma-ray linear counting rates. The consequences were weaker ^{111}Ag source strengths, longer counting times per experiment, and resultant poorer statistics, as compared to the ^{181}Hf experiments. Fortunately, the longer half life allows the perturbation to be followed over several cycles, which compensates to some extent for the poor statistics. In addition, as the finite time resolution (FTR) of the electronic apparatus is only ~5% of the half life of the intermediate nuclear state in ^{111}Cd (versus ~38% in ^{181}Ta), the data is less sensitive to the smearing and damping effects of the FTR. In fact, the early least-squares analysis was done ignoring FTR in order to significantly reduce computational times. All final fits, however, were made considering the FTR as described in COO-3246-15.

The theory as presented in section A does not suffice to describe the potential situations in solutions of macromolecular species. The possibility

for a time dependent interaction is very high. Briefly, if the nuclear quadrupole moment interacts with a time dependent EFG (i.e., fluctuating EFG's due to ions moving in the solution), the interaction may be described by relaxation

$$G_{kk}(t) = \exp[-\lambda_k t] \tag{4}$$

The relaxation parameter is related to the quadrupole frequency, ω_q and the average time between interactions or correlation time, τ_c by

$$\lambda_k = 3/5\ \tau_c \omega q^2\ \{k(k+1)[4I(I+1) - k(k+1) - 1]\} \tag{5}$$

For solutions of macromolecular species, τ_c is replaced by the rotational diffusion time

$$\tau_R = \frac{4\pi a^3 \eta}{3kT} \tag{6}$$

where a is the molecular radius, η the solvent viscosity, and T the absolute temperature. The k in equation (6) is the Boltzmann constant and is different from the summation constant in equations (4) and (5). For $k = 2$, τ_R equals τ_2.

As the macromolecules will be studied in solution, the feasibility of combined static and time dependent interactions arises. If the interaction results from a single nucleus experiencing a static interaction due to the binding site electronic structure as well as relaxation due to rotational diffusion, the perturbation coefficient would be a multiplicative combination of equations (1) and (4). If the interaction results from two different sites, one static and the other time dependent, the $G_{22}(t)$ is given by the addition of equations (1) and (4) with appropriate weighting factors.

Before proceeding to the experiments on the macromolecular species, both TDPAC and IPAC (integral perturbed angular correlations) experiments were performed on dilute solutions of $^{111}AgNO_3$, in order to test the system for any extraneous perturbations due to the contaminant, ^{110m}Ag. Both experiments

should give the fully unattenuated value for the angular correlation coefficient, A_{22}. The predicted value for A_{22}[24] for the silver cascade of [3/2 (M1) 5/2 (Q) 1/2] is -0.20, with A_{44} equaling zero. The results for both experiments are given in Fig. 5. The result of averaging the TDPAC spectrum ($A_{22}\overline{G_{22}(\infty)}$)over the first 40 nsec (solid line) gave an A_{22} value of -0.195 $\pm$ 0.021. The value has been corrected for the solid angles subtended by the detectors and any system nonlinearities. The IPAC data given at the bottom of Fig. 5 was least-squares fit to the standard angular correlation function,

$$W(\theta) = \sum_{k=0,2,4} A_{kk} P_k (\cos \theta),$$

where P_k (cos θ) is a Legendre polynomial. The resulting fit parameter for A_{22}, after application of all corrections and normalization to A_{oo} = 1.0, was A_{22} = -0.212 $\pm$ 0.017. Both experiments conclusively proved that the system was free of extraneous perturbations and our application of the correction techniques were appropriate.

2. Nuclear Quadrupole Interactions of ^{181}Hf in Vitamin B_{12}.

Cyanocobalamine or Vitamin B_{12} (MW = 1355 daltons) is a naturally occurring Co(III) containing enzyme. The cobalt ion is in a porphyrin-like ring coordinated by four nitrogen atoms in a plane, with the fifth position filled by an adenine nitrogen and the sixth position of the octahedron by a CN^- ion. The complex exhibits a diamagnetic ground state[25] (see the center of Fig. 6 for the structure of Vitamin B_{12}). The phosphate binding site located on the side arm of the porphyrin ring was chosen as the preferential site for the binding of ^{181}Hf nuclei, with one hafnium atom per B_{12} molecule. The resulting complex was studied in the solid and aqueous forms.

Vitamin B_{12} was obtained from Research Plus Laboratories, Inc. ^{181}Hf activity was transferred to a nearly saturated solution of Vitamin B_{12} in approximately 2 ml of solution. Vitamin B_{12} will always be in excess to the

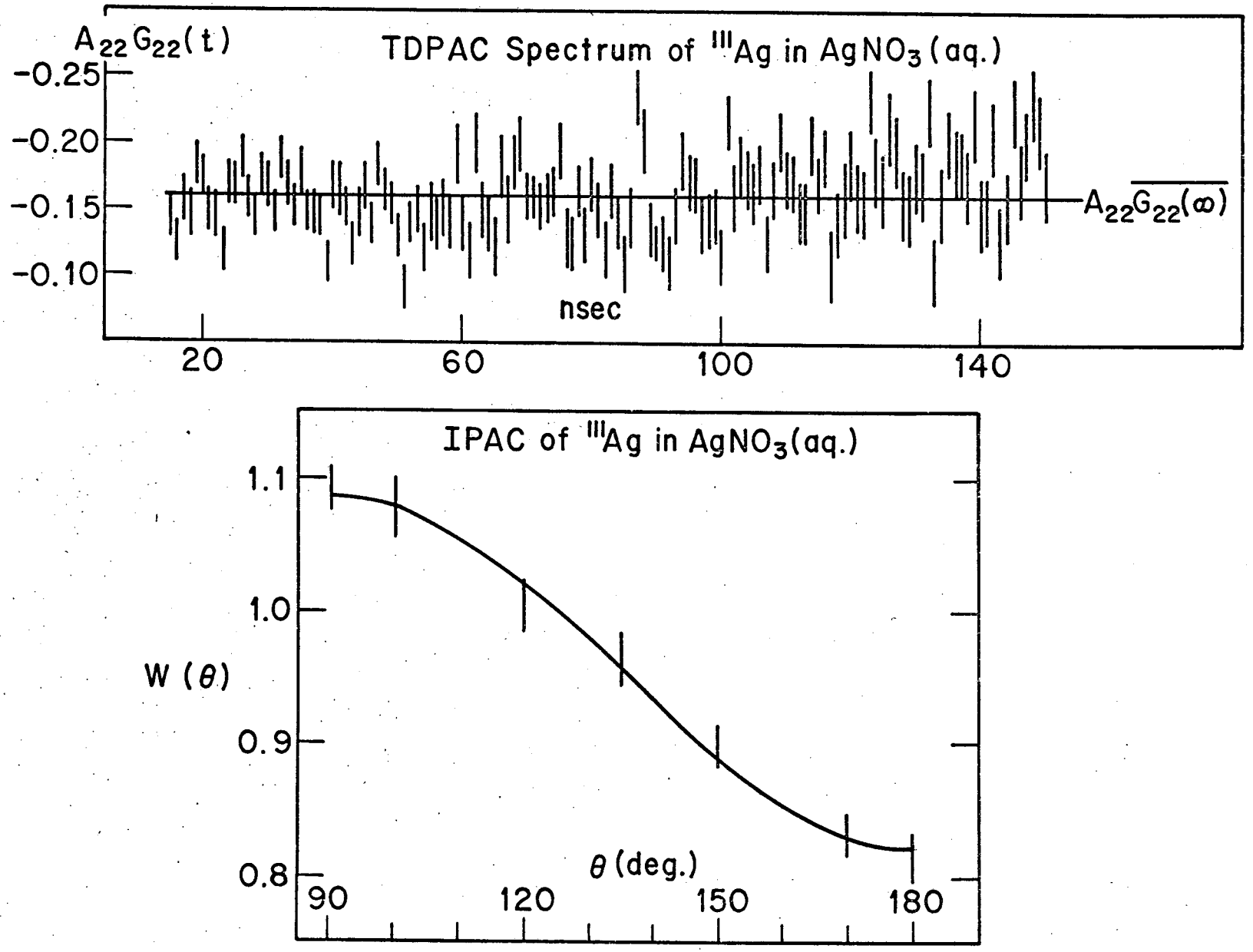
TDPAC Spectrum of ^{111}Ag in $AgNO_3$ (aq.)
$A_{22}G_{22}(t)$
-0.25
-0.20
-0.15
-0.10
$A_{22}\overline{G_{22}(\infty)}$
nsec
20
60
100
140
IPAC of ^{111}Ag in $AgNO_3$(aq.)
1.1
1.0
0.9
0.8
W (θ)
θ (deg.)
90
120
150
180

Figure 5.

hafnium. Acetone was added dropwise until the solution exhibited heavy cloudiness. After the addition of 5 ml more acetone, the solution stood covered at room temperature for 12 hours. The volume ratio of B_{12} solution to acetone was approximately 1 to 8. The resulting precipitate was vacuumed filtered and air dried. The above procedure[26] was repeated using the precipitate obtained from the first crystallization. The liquid sample of hafnium-B_{12} was obtained by dissolution of the twice precipitated solids.

In order to ascertain the nature of the hafnium-B_{12} bond, both a tracer experiment and ^{31}P NMR were performed on the complex. Using a 1:1 molar ratio of Hf:B_{12} solution, tagged with ^{181}Hf, an acetone crystallization was performed. The disposition and amount of hafnium was determined by NaI counting and the amount of Vitamin B_{12} was determined by weighing the resulting precipitate. It was found that ~35% of the radioactivity precipitated with ~31% of the original B_{12} in solution. Therefore, it was concluded that only one Hf nucleus is associated with each B_{12} molecule, indicative of a single binding site.

The binding of hafnium to oxygens of the B_{12} phosphorous atom would be reflected by a ^{31}P NMR experiment. Samples of native Vitamin B_{12} and the Hf-B_{12} complex were analyzed by Dr. R. Rowan and Dr. S. O. Grim at the University of Maryland NMR facility. On the addition of Hf, the single sharp resonance line typical of the native sample, was converted to 4 very broad resonances with the major peak occurring in nearly the same field position as in the native sample. The remaining broadened peaks were chemically shifted by approximately 2.2, 6.7, and 9.2 ppm upfield. The broadening was attributed to the influence of the hafnium isotopes' quadrupole moments, whereas the small chemical shifts are best explained by varied changes in the π bonding electron density at the phosphorous. If a single hafnium attaches itself to the phosphorous oxygens and then acquires further (and varied) oxygen bonds by

hydrolysis with water molecules, the degree of π bonding to the oxygens of the B_{12} phosphorous would vary. The resulting picture for the aqueous complex is one of several Hf-O-P species distinguished by slightly varying π bonding (and therefore electron density) at the ^{31}P atoms and varied numbers of bound water molecules. It was assumed that the solid complex would be similar with a varied number of waters of hydration at the hafnium nucleus.

The TDPAC spectra for the solid and aqueous solution of the Hf-B_{12} complex is given in Fig. 6. In order to facilitate the complete understanding of the experimental conclusions, a qualitative analysis of the data will be presented prior to the presentation of the least-squares analysis. The arrow to the right of each spectrum is the measured value for $A_{22}\overline{G_{22}(\infty)}$, as obtained in an IPAC experiment.

The immediate conclusion to be drawn about the solid Hf-B_{12} complex (top of Fig. 6) is that the hafnium nuclei are tightly bound to the B_{12} molecule and are experiencing a static nuclear quadrupole interaction which is strongly damped. The aperiodic positioning of the maxima and minima, as well as the significant amplitude damping, is indicative of one or possibly a combination of the following; a large frequency distribution or else the destructive addition of spectra originating from several different binding sites, a non-axially symmetric EFG or finally, the possibility of source orientation which would produce curves strongly uncharacteristic of polycrystalline sources.

The solution data, given at the bottom of Fig. 6, is most surprising. Not only does the hafnium remain bound to the B_{12} but it seems to display nearly the same interaction as the solid source. A much stronger, but different, damping influence is operative which can possibly be explainable in terms of the influence of free ions in solution as the large molecule rotates (rotational diffusion). The drop-off trend is indicative of a time dependent

Figure 6.

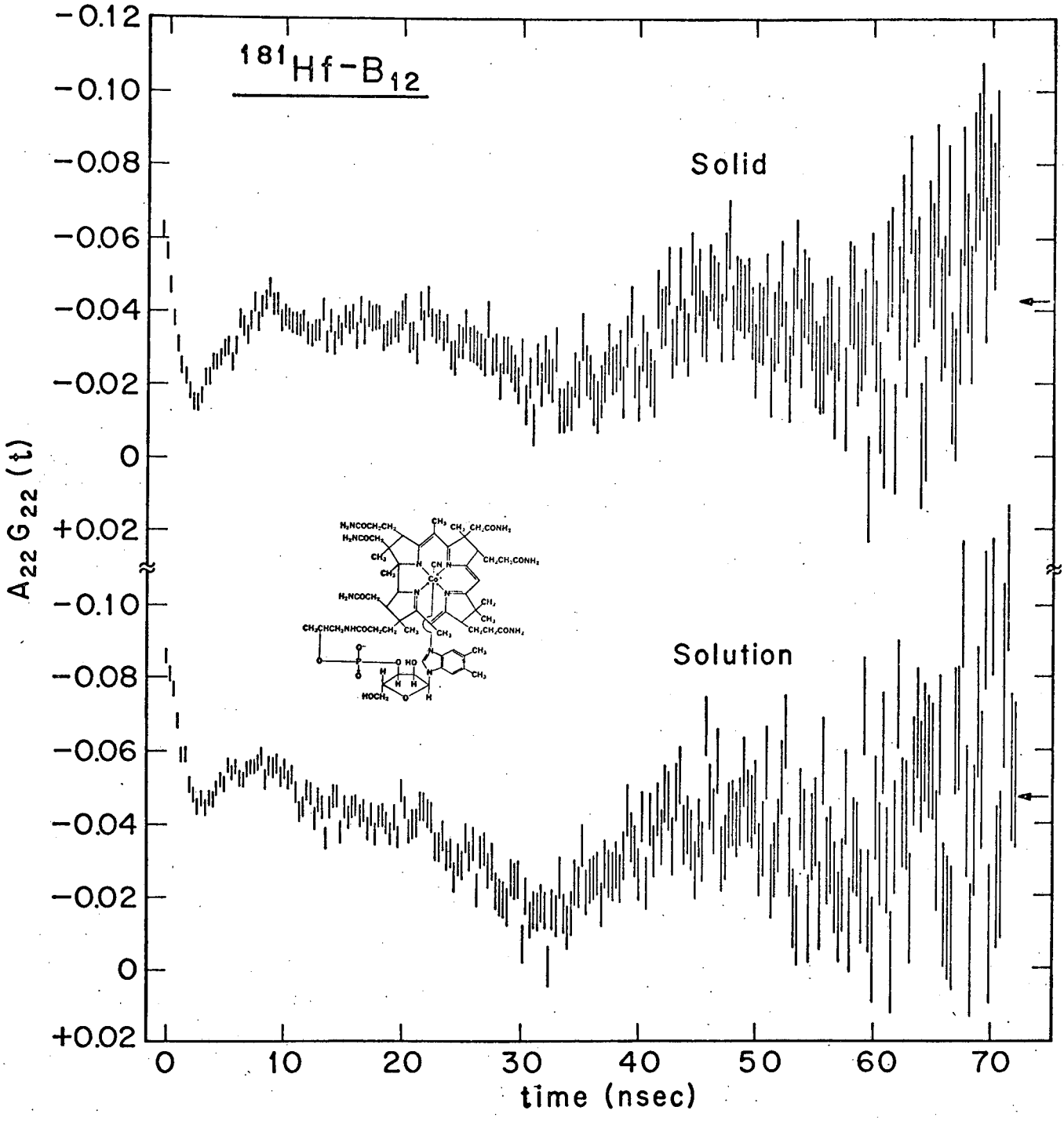
$^{181}Hf-B_{12}$
Solid
Solution
$A_{22}G_{22}(t)$
time (nsec)
-0.12
-0.10
-0.08
-0.06
-0.04
-0.02
0
+0.02
0
10
20
30
40
50
60
70

interaction with a short correlation time, which is present in addition to the static interaction.

The qualitative information led us to try least-squares fits of the data to several functional forms for the perturbation coefficient. They included (1) a single nuclear quadrupole interaction coupled with rotational diffusion (multiplicative combination of a static and a time dependent interaction); (2) additive combination of time dependent and static effects; and (3) more than one binding site (and therefore interaction frequency) with and without multiplicative or additive time-dependent effects. In none of these cases were the fits appropriate at long times but the trends at the earlier times could be reproduced fairly well. In all fits concerning two distinct interaction sites, no convergence to the data was obtained. This could, however, be an artifact of our fitting procedures coupled with the lack of fine structure evident in the data.

The experimental data for the crystalline sample was best fit to a single quadrupole frequency with a relatively large frequency distribution. The computed fit is shown as the solid curve in the upper half of Fig. 7. The derived fit parameters are:

$$\omega_1 = 378 \pm 35 \text{ MHz}$$

$$\omega_2 = 798 \pm 112 \text{ MHz}$$

$$\delta = 0.184 \pm 0.082$$

(Note: the large errors reflect the poor fit at long times.) Within the error of the experiment, the asymmetry parameter was zero and the following quadrupole frequency and EFG parameters result:

$$\omega_q = 63 \pm 6 \text{ MHz}$$

$$|V_{zz}| = (6.77 \pm 0.65) \times 10^{17} \text{ V/cm}^2$$

$$|V_{yy}| = |V_{xx}| = (3.39 \pm 0.40) \times 10^{17} \text{ V/cm}^2.$$

The above values reflect the error in ω_1 only. The magnitude of the EFG is

Figure 7.

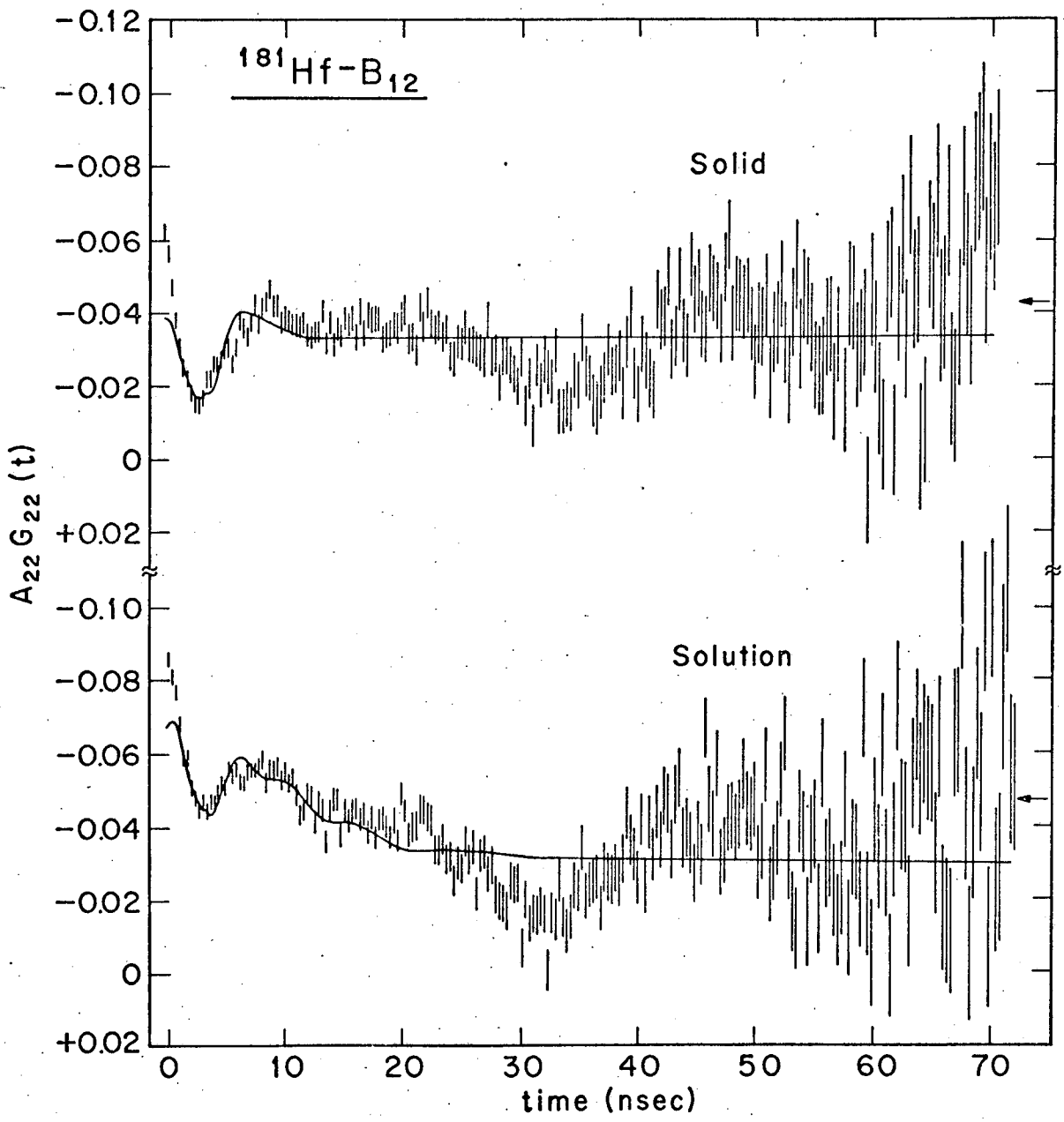
$^{181}Hf-B_{12}$
Solid
Solution
$A_{22}G_{22}(t)$
-0.12
-0.10
-0.08
-0.06
-0.04
-0.02
0
+0.02
0
10
20
30
40
50
60
70
time (nsec)

similar to the values obtained for the pyrophosphate and diphosphate hafnium species. The large δ is typical of hafnium compounds involving waters of hydration.

Considering the large plate-like structure of the B_{12} molecule, orientation in the solid state was expected. This assumption was confirmed by an investigation of the values obtained for the coefficients, S_{kn}. On comparing our least-squares fit values, one found that all coefficients significantly differed from those that would have been exhibited by a source experiencing a randomly oriented static EFG.

The best approximation to the liquid data was obtained by assuming that the large majority of the hafnium atoms experienced a static electric quadrupole interaction with a set frequency distribution of 18%, while a small percentage of the hafnium atoms are released into solution and exhibit a time dependent relaxation behavior. The calculated curve which results is shown in the lower half of Fig. 7. The fit parameters for the bound hafnium species are

$$\% = 76.1 \pm 0.9$$

$$\omega_1 = 460 \pm 20 \text{ MHz}$$

$$\omega_2 = 721 \pm 31 \text{ MHz}$$

The resulting η of 0.48 ± 0.07 gives the following

$$\omega_q = 62.6 \pm 4.1 \text{ MHz}$$

$$|V_{zz}| = (6.73 \pm 0.44) \times 10^{17} \text{ V/cm}^2$$

$$|V_{yy}| = (4.98 \pm 0.80) \times 10^{17} \text{ V/cm}^2$$

$$|V_{xx}| = (1.75 \pm 0.28) \times 10^{17} \text{ V/cm}^2$$

The only major change to those hafnium which remained bound on dissolution of the solid complex is an increase in the asymmetry parameter of the EFG. Considering the experimental error, this is not conclusive. As in the solid complex, the fit values for the S_{kn} coefficients, even though the errors were large, tended to indicate the presence of orientation of the EFG at the Hf

binding site.

The hafnium species which were released to the solution, exhibited the following

$$\% = 23.9 \pm 0.9$$

$$\lambda_2 = (1.21 \pm 0.20) \times 10^8 \text{ sec}^{-1}$$

Using typical hafnium quadrupole frequencies in the range of $\sim 6 \times 10^7$ to 1.2×10^8 Hz, one calculates employing equation (5), a range of correlations times (τ_c) from 3×10^{-10} to 8×10^{-11} sec. Using equation (6) and solving for the molecular radius, a, one arrives at the conclusion that the hafnium relaxation behavior originates from species about 4-6 Å in radius. This size and behavior would be typical of a largely hydrolyzed hafnium atom, which had formed after release from a B_{12} binding site.

Certain conclusions can be drawn concerning the B_{12} molecule itself, in addition to the previously presented conclusion on the hafnium-B_{12} binding site. Both the solid and liquid data indicated that the B_{12} molecule is a highly oriented species even in low-viscosity liquids. Because the hafnium nuclear quadrupole interaction was relatively free of effects due to rotational diffusion, it can be concluded that the size and orientation of the B_{12} molecule force it to form a fairly highly "structured" solution. This conclusion is further supported by the retention of the "solid-like" characteristic of the nuclear quadrupole interaction in solution.

3. Nuclear Quadrupole Interactions of Two Metal-DNA Complexes

The nuclear quadrupole interactions of deoxyribonucleic acid (DNA) as experienced by ^{181}Ta and ^{111}Cd intermediate nuclear states were explored as a function of temperature and physical state. The chemical properties of a hafnium-DNA complex were unknown but it was assumed that it would bind preferentially to the phosphate oxygens along the backbone of the DNA helix. The

possibility for additional binding to the abundant oxygens bound to the backbone carbons could not be excluded. In either site, the hafnium would be situated on the outer surface of the DNA molecule and should therefore be sensitive to the rotational diffusion properties of the DNA. On the other hand, the binding of silver (^{111}Ag) to DNA has been established by several groups.[27-29] The silver ion binds preferentially to the purine bases (adenine and guanine), with the N-7 of quanine being the preferred site. The binding of silver does not disrupt the regular Watson-Crick structure of the DNA helix.[27] The location on the "interior" of the helix should reduce the sensitivity of the silver interaction to the rotational diffusion of the macromolecule (in comparison to hafnium). Therefore, the two complexes with DNA offer a view of the "outside" and "inside" of the DNA double helix, which will provide a more complete picture of the behavior of DNA as a whole.

A highly polymerized calf-thymus DNA was obtained from ICN Biochemicals (Life Sciences Group). The sample is reported to be a native sample (double stranded) of reasonably high molecular weight with a phosphorous content of 7.3% by bottle weight[27] and an intrinsic viscosity, $[\eta]$, of 7×10^3 ml/g.[27,30] The following procedure was used for the hafnium-DNA samples. ^{181}Hf activity was combined with a small amount of $HfOCl_2$ solution (< 1 mg/ml) and then neutralized with 1 N NaOH. DNA was slowly dissolved in distilled water to produce a viscous solution of a concentration of ~0.05 g/ml. The two solutions were then combined with gentle stirring and transferred to Spectrapor membrane tubing (M.W. cutoff: 12,000-14,000; 25 mm) for dialysis against water. The dialysis proceeded for at least 24 hours with frequent changes of the water in the dialysis bath. The pH of the final solutions were ~6-7. Samples were stored in cylindrical glass ampoules and sealed against water loss. The complex involving one Ag^{+1} ion per DNA molecule forms only for molar ratios (r_b) of

moles of bound Ag^+ to moles of DNA of less than 0.2. For each sample, a known weight of DNA was dissolved in 0.10 M $NaClO_4$ giving a final pH of 5.6, and the moles of DNA in terms of phosphate were calculated. Depending on the DNA sample size ($\sim 10^{-4}$ moles in terms of phosphate), the appropriate amount of $^{111}AgNO_3$, after neutralization with NaOH, was added dropwise (with gentle stirring) to the DNA-$NaClO_4$ solutions. The final solutions were $\sim 10^{-3}$-10^{-4} molar in phosphate and exhibited very high viscosities, indicative of a high molecular weight product. TDPAC experiments were performed at various temperatures between -50°C and +80°C employing the gas flow heat-freeze system described previously in COO-3246-15.

The DNA-Hf species were studied at -50°C corresponding to a solid state and at 25°C in the liquid state. No damage to the DNA helical structure is expected on freezing. Both TDPAC spectra are given in Fig. 8.

The top half of Fig. 8 gives the data for the DNA solution at -50°C, which is best considered as solid material and was fairly well represented by a single static quadrupole interaction. The fit (solid line) yielded the following parameters

$$\omega_1 = 505 \pm 49 \text{ MHz}$$

$$\omega_2 = 1001 \pm 34 \text{ MHz}$$

$$\eta = 0.08 \pm 0.32$$

$$\delta = 0.07 \pm 0.03$$

The resulting asymmetry parameter was taken to be zero in light of the large error, and the following results.

$$\omega_q = 84.2 \pm 8.2 \text{ MHz}$$

$$|V_{zz}| = (8.72 \pm 0.85) \times 10^{17} \text{ V/cm}^2$$

$$|V_{yy}| = |V_{xx}| = |V_{zz}|/2 = (4.36 \pm 0.42) \times 10^{17} \text{ V/cm}^2$$

Figure 8.

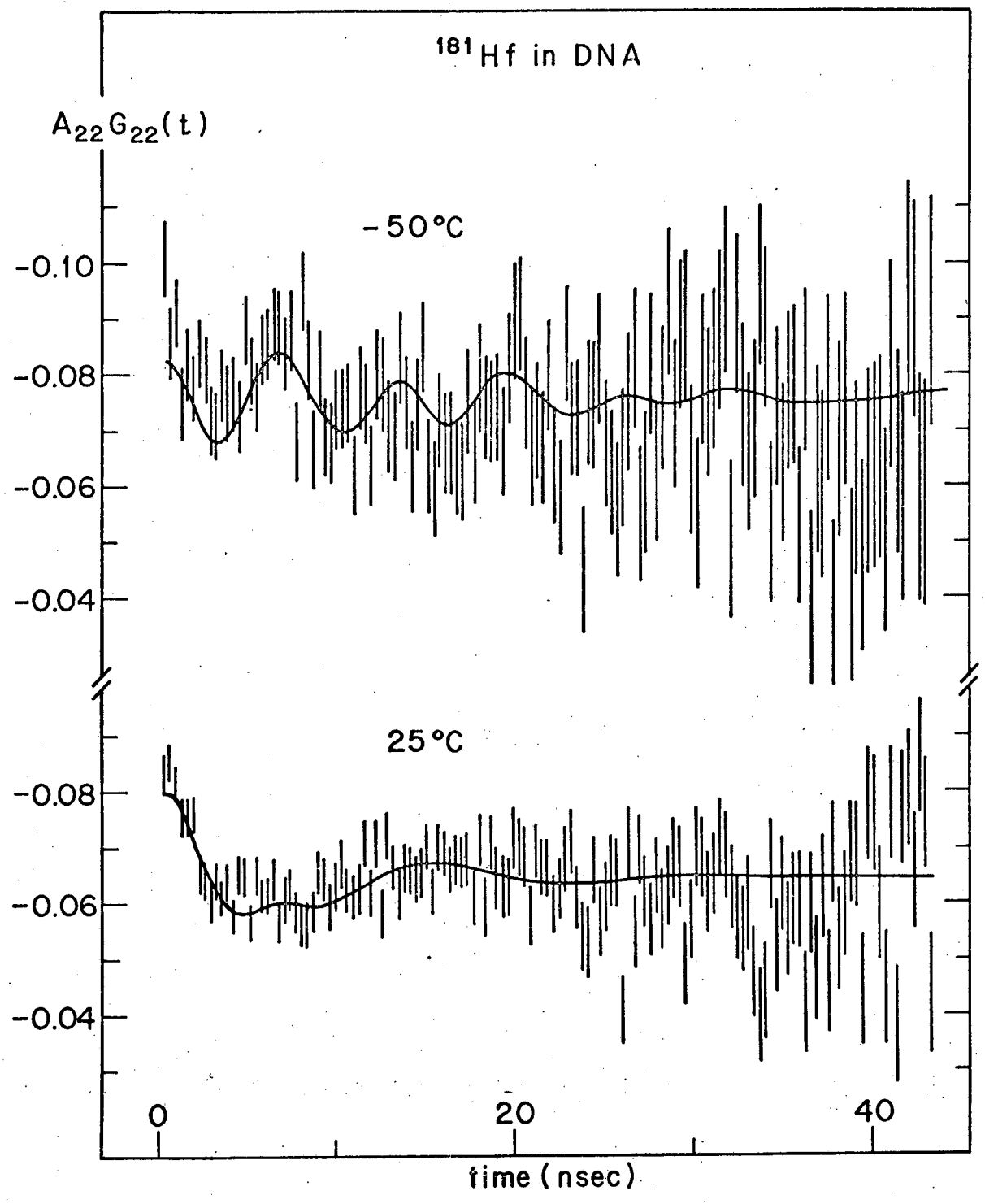
^{181}Hf in DNA
$A_{22}G_{22}(t)$
-50°C
-0.10
-0.08
-0.06
-0.04
25°C
-0.08
-0.06
-0.04
0
20
40
time (nsec)

The room temperature data is given at the bottom of Fig. 8. As would be expected for a liquid state, the interaction is more strongly damped at 25°C but it still maintains its "solid-like" characteristics. The large damping effect prevented the accurate determination of ω_2 and ω_3 and therefore η. The interesting feature is the quite evident change in the magnitude of the quadrupole frequency as revealed by the least squares fit.

$$\omega_1 = 412 \pm 32 \text{ MHz}$$

$$\omega_2 = 753 \pm 481 \text{ MHz}$$

For an asymmetry parameter of zero, one obtains

$$\omega_q = 68.7 \pm 5.3 \text{ MHz}$$

$$|V_{zz}| = (7.14 \pm 0.55) \times 10^{17} \text{ V/cm}^2$$

$$|V_{yy}| = |V_{xx}| = (3.57 \pm 0.28) \times 10^{17} \text{ V/cm}^2$$

If η is greater than zero, the ω_q would be reduced below the above value, confirming that the quadrupole frequency has been significantly changed by the temperature and phase change. The frequency distribution for the 25°C case was $\delta = 22 \pm 6\%$. This large increase may be partially due to the rotational diffusion of the molecule but in all likelihood originates mainly from the increased hydrolysis of the hafnium nucleus in the aqueous case.

Extensive fitting to multiplicative combinations of time dependent and static interactions, revealed that the hafnium interaction is essentially insensitive to the rotational diffusion of the DNA. This indicates that the hafnium nuclei are shielded from the free ions in solution by either the DNA molecule itself or by a large hydrolysis sphere. A lack of evidence for rotational diffusion effects also indicates that the DNA in these viscous solutions is rotating very slowly.

Neither the least-squares analysis of the S_{kn} coefficient or the results of IPAC experiments (i.e., $A_{22}S_{20} \simeq A_{22}\overline{G_{22}(\infty)}$) provided any strong evidence for

the molecular orientation of the EFG. Though the error was high on these parameters (S_{kn}'s and $A_{22}\overline{G_{22}(\infty)}$), it was concluded that the phosphate binding sites exhibit randomly oriented EFG's.

The decrease in the quadrupole frequency with increasing temperature most likely corresponds to a decrease in the degree of π bonding between hafnium and the oxygens of the molecules in the "hydrolysis sphere". At -50°C, the inherent greater rigidity and reduced molecular motion would imply an increased π bonding to the oxygens than that exhibited by the liquid state. However, as the solid nature of the sample is not lost on going to the solution, the bonding may be envisioned as the same as that in the solid state but with an increased "wobbliness" in the hafnium-oxygens bonds which is reducing the π structure.

The study of DNA using a hafnium label indicated that significant changes were occurring on the "outside" of the DNA helical structure as a function of the temperature. The use of silver will allow the investigation of the "inside" of the molecule as the environment is changed. In addition, the smaller size of the Ag^+ ion and the known chemistry in DNA frees the interpretation of the data from the uncertainty concerning the origin of the interaction. The solutions were studied at four temperatures, -50°C, 25°C, 40°C, and 80°C. The last temperature is above the predicted helix coil transition temperature (T_m) of ~77° for these samples[31] and corresponds to the denatured molecule. The same sample was used for both the frozen and room temperature experiments, the former being performed initially. The two experiments performed at higher temperatures (+40° and +80°C) employed separate samples, as the effects on the DNA of high temperatures over extended periods was unknown. The examination of the +40° sample after completion of the experiment indicated that neither denaturation or degradation had occurred. The higher temperature sample was much less viscous after heating indicating a

significant loss in molecular weight and contained a grayish black precipitate, which is believed to be a mixture of denaturation products (small amino acid chains). The activity was equally distributed throughout both the solution and the precipitate.

The data for all four temperatures, along with the final least-squares fits (solid lines) are given in Fig. 9. The 80° data exhibited such large scatter that no fit was obtainable. This can be attributed to both the greater molecular motion expected for the lower viscosity solution and the greater exposure of the guanine binding sites to said motion due to the denaturation. It also could reflect the release of Ag^+ into solution, though this should exhibit a strong time dependent component. The data seems to be fairly constant around a value of ~ -0.07 indicative of a strongly damped static interaction. The results for the quadrupole frequencies, resulting η's and the electric field gradient components are tabulated in Table II. The only sample which exhibited a significant attenuation due to a distribution in frequencies was the room temperature data. It amounted to ~5%. None of the experiments were approximated by including either multiplicative or additive time dependent effects. It is interesting and surprising to note that the quadrupole interaction in DNA is not changing with temperature. There seems to be a slight decrease in the ω_q for the 40° data and the asymmetry parameter has definitely increased. Otherwise, the interaction is insensitive to changes in temperature. This seems to indicate that the DNA molecule is a very compact entity in solution even at relatively high temperatures. Any uncoiling of the DNA helix would have been evidenced by increased time dependent effects as the temperature increases.

It is obvious immediately from an inspection of the ^{111}Ag-DNA values for the limiting time integral result, $A_{22}\overline{G_{22}(\infty)}_{lim}$ that the sources are not

Figure 9.

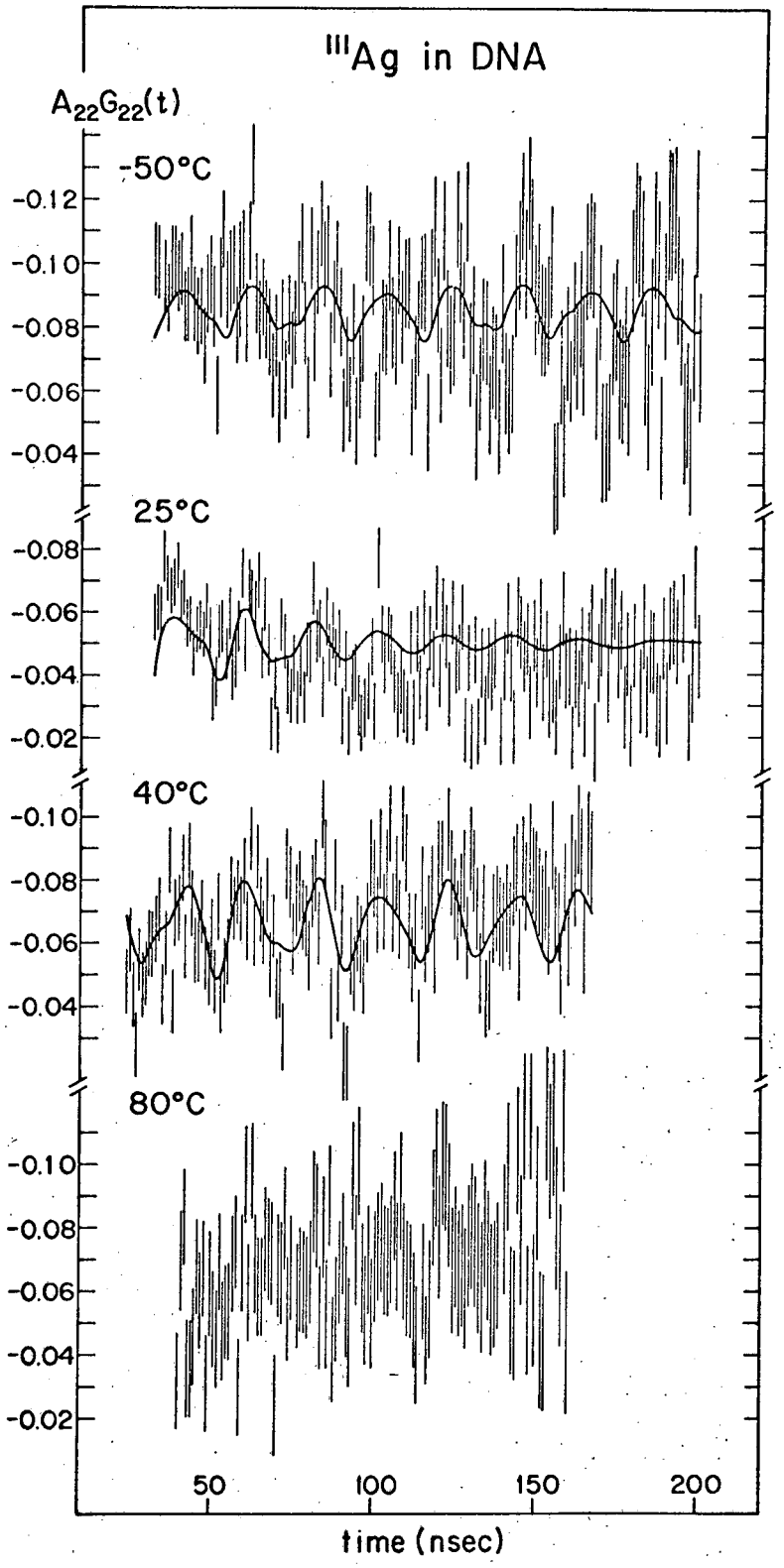
^{111}Ag in DNA
$A_{22}G_{22}(t)$
-50°C
-0.12
-0.10
-0.08
-0.06
-0.04
25°C
-0.08
-0.06
-0.04
-0.02
40°C
-0.10
-0.08
-0.06
-0.04
80°C
-0.10
-0.08
-0.06
-0.04
-0.02
50
100
150
200
time (nsec)

Table II. Parameters Describing the Nuclear Quadrupole Interactions of ^{111}Ag in DNA Solutions

Sample Temperatures	ω_q	η	Electric Field Gradient Components in 10^{18} V/cm^2* $\lvert V_{zz}\rvert$	$\lvert V_{xx}\rvert$	$\lvert V_{yy}\rvert$
-50°C	44.27 ± 0.76	0.38 ± 0.03	1.94 ± 0.37	0.604 ± 0.125	1.340 ± 0.280
25°C	45.57 ± 1.39	0.37 ± 0.04	2.00 ± 0.38	0.630 ± 0.138	1.369 ± 0.300
40°C	42.22 ± 0.56	0.47 ± 0.02	1.85 ± 0.35	0.496 ± 0.096	1.358 ± 0.263

*The error on the electric field gradient components contain both the error in ω_q and the large uncertainty in the electric quadrupole moment, Q.

representative of a randomly oriented EFG. The fit values for $A_{22}S_{20}$ for ^{111}Ag-DNA and the predicted random result for various source-to-detector distances, H, have been tabulated and compared in Table III. Investigation of the remaining coefficients should further support the existence of orientation, as well as reveal possible changes with temperature. In order to remove all solid angle effects, system nonlinearities and dependence on the A_{22} parameter, the coefficients have been normalized to $S_{20} = 1.0$. The comparison has been made in Table IV. The large error on the S_{23} coefficient prevented its use for any valid conclusions. The DNA samples at all temperatures exhibit values of the coefficients differing in magnitude and/or sign from the randomly oriented EFG result. The samples exhibited a much larger isotropic component, $A_{22}S_{20}$, as well. The only significant change among the samples themselves occurs between -50°C and 25°C as would be anticipated for the phase change occurring. The remaining temperatures exhibit little change as evidenced by the nearly constant value for S_{21}, the second best determined coefficient.

In summary, the ^{111}Ag-DNA data definitely indicates changes in molecular orientation with phase and temperature. This fact is not in any way contradicted by the constancy of the quadrupole frequency, as the frequency of the

Table III. Comparison of $A_{22}S_{20} \simeq A_{22}\overline{G_{22}(\infty)}_{lim}$ for the ^{111}Ag-DNA samples to the result expected for a randomly oriented EFG at various source-to-detector distances, H.[2]

Sample Temperature	H (cm)	$A_{22}S_{20}$
-50°C	10	-0.0872 ± 0.0087
+25°C	5	-0.0514 ± 0.0436
+40°C	6	-0.0775 ± 0.0112
+80°C	6	-0.07 ± 0.02
Randomly	5	- .0322
Oriented EFG	6	- .0338
Results	10	- .0372

Table IV. Values of the Normalized Coefficients, S_{2n}, for ^{111}Ag in DNA Solutions at Various Temperatures

Sample Temperature	S_{20}	S_{21}	S_{22}	S_{23}
-50°C	1.0	0.94 ± 0.34	0.34 ± 0.40	-0.023 ± 0.137
25°C	1.0	0.28 ± 0.36	0.28 ± 0.40	-0.25 ± 1.13
40°C	1.0	0.19 ± 0.06	-0.096± 0.060	0.026 ± 0.208
Randomly Oriented Result	1.0	1.86	1.43	0.714

interaction is independent of the orientation. The constancy of η for the two temperatures -50°C and 25°C is inconclusive. The molecular orientation could easily change in such a way that the Ag-nitrogen bond retains the same charge distribution and symmetry. Likewise, the increase in η between the 25°C and 40°C data cannot be attributed directly to any change in molecular orientation, nor does the change invalidate any conclusions concerning orientation. Overall, the DNA molecule is a highly oriented species which even in solution is best

approximated by solid-like characteristics, as seen from the point of view of ^{111}Ag (^{111}Cd) nuclei.

4. Relation Between the Two Labelled DNA Species

The results for the study of DNA labelled with ^{181}Hf and ^{111}Ag should be compared and correlated in order to derive an overall view of the DNA in solution. The hafnium experiments indicated that the "outside" of the DNA molecule undergoes quite significant changes between the solid and liquid states, was relatively nonoriented, and was best approximated by a polycrystalline species in solution, rather than a freely moving ion. It should be noted, though, that the binding of a heavy atom such as hafnium which in turn, forms an even larger ion through hydrolysis, could significantly change the DNA structure at the binding site and such parameters as the magnitude of ω_q and η could be only measures of hafnium properties and not those of DNA in its natural state. The lack of orientation and the over-all solid behavior of the molecule are definitely characteristic of the DNA. Tagging with silver guarantees the study of a known site in the DNA, as well as the knowledge that the Watson-Crick structure is not being disrupted. Therefore, the conclusions from this study should apply directly to the DNA molecule. The "inside" of the DNA molecule also exhibits a polycrystalline solid behavior in solution even at relatively high biological temperatures. However, in contrast to hafnium, the silver-DNA species exhibited significant orientation, as well as different orientations, as a function of temperature and phase. In order for the DNA double helix to form, every base pair along the inside of the helix must be exactly oriented with respect to the other base pairs. This high degree of symmetry throughout the molecule is necessary in order to guarantee the correct hydrogen bonding between the individual base pairs and their correct stacking arrangement along the length of the molecule. The resulting molecule will exhibit a high symmetry and regularity that could easily result in a net preferred direction for the

EFG at the nitrogens. The silver atom sitting in the interior of the molecule would be extremely sensitive to the orientation. The "outside" or backbone of the double helix, however, should not require such a great degree of orientation throughout the entire length of the molecule, especially at the two Hf binding site oxygens of the phosphates which are not directly bound to the superstructure of the DNA molecule and should have a larger number of degrees of motional freedom. Their particular orientation in space is not exactly fixed and the orientation at one site will not necessarily exhibit the same orientation as another site along the backbone. Therefore, the net result would be a randomly oriented set of microcrystals.

The persistence of the solid state behavior for both labelled DNA's should also be considered. If one accepts the Watson-Crick structure for DNA and the resulting symmetry on the interior of the helix, the non-free ion nature of the silver-DNA in these highly viscous solutions is fairly easy to understand. In the hafnium-DNA case, there was no direct evidence for a rotational correlation effect either. This seems to imply that the majority of the phosphate-hafnium binding sites are shielded from the free ions in solution either by the formation of quite large hydrolysis species at the hafnium or because the DNA molecule is folded over onto itself. The former source of shielding would not be expected to be so excellent a shielder that no effects are discernible. The folding and wrapping of the molecule could very easily lead to the complete protection of the hafnium binding sites, with a few sites located on the perimeter of the folded molecule which would produce only a small damping effect (i.e., the increased δ for the room temperature hafnium data). If the molecule does wrap around itself (envision a coiled up snake) in solution, the molecular radius could be quite large producing such a large τ_R that many cycles of the nuclear quadrupole interaction would occur during one

rotation of the DNA molecule. Consequently, the interaction of both the silver and hafnium would be insensitive to the rotational correlation time. Summing up, the TDPAC experiments indicate that DNA exhibits a highly oriented inner structure with a more randomly oriented outer surface. It also seems to exhibit essentially solid-like characteristics in high viscosity solutions, even at elevated temperatures.

References

1. Table of Isotopes, 6th Edition, ed. by C. M. Lederer, J. M. Hollander and I. Perlman, J. Wiley and Sons, Inc., New York, 1967.

2. H. Frauenfelder and R. M. Steffen, "Angular Correlations" in "Alpha-, Beta-, and Gamma-Ray Spectroscopy", Vol. 2, ed. by K. Siegbahn, North-Holland Publishing Co., Amsterdam, 1965.

3. Calculated using the equations given in E. Gerdau, J. Wolf, H. Winkler, and J. Braunfurth, Proc. Roy. Soc. A311, 197 (1969).

4. Nuclear Data Sheets 9, 337 (1973).

5. W. B. Blumenthal, "The Chemical Behavior of Zirconium", D. Van Nostrand, Inc., Princeton, New Jersey, 1958.

6. G. Marest, I. Berkes, G. Bougnot, and R. Béraud, C. R. Acad. Sci. Paris 262, Series B, 367 (1966).

7. P. R. Gardner and W. V. Prestwich, Can. J. of Phys. 48, 1430 (1970).

8. L. Gordon, M. L. Salutsky, and H. H. Willard, "Precipitation from Homogeneous Solutions", J. Wiley and Sons, Inc., New York, 1959, p. 49.

9. L. Mayer, E. Bodenstedt, and C. Günther, Z. Physik 177, 28 (1964).

10. J. A. Cameron, P. R. Gardner, L. Keszthelyi, and W. V. Prestwich, Chem. Phys. Lett. 4, 229 (1969).

11. E. N. Kaufmann, Phys. Rev. B4, 1382 (1963) and Phys. Rev. B4, 1387 (1963).

12. M. Forker, J. B. Fechner, and H. Haverkamp, Z. Physik 269, 279 (1974).

13. T. K. Leipert, J. D. Baldeschweiler, and D. A. Shirley, Nature 220, 907 (1968).

14. C. F. Meares, R. G. Bryant, J. D. Baldeschweiler, and D. A. Shirley, Proc. Nat. Acad. Sci. 65, 1155 (1969).

15. D. A. Shirley, J. Chem. Phys. 53, 465 (1970).

16. D. A. Shirley, J. Chem. Phys. 55, 1512 (1971).

17. R. Bauer, P. Lumkilde, and O. Glomset, Phys. Rev. Lett. 32, 340 (1974).

18. L. Richer, G. Graf, and J. Glass, J. Chem. Phys. 61, 396 (1974).

19. F. Sicilio, M. D. Peterson, and G. G. Rudolph, Anal. Chem. 28, 365 (1956).

20. J. J. Behrend and D. Budnick, Z. Physik 168, 155 (1962).

21. E. Bodenstedt, U. Ortabasi, and W. H. Ellis, Phys. Rev. B6, 2909 (1972).

22. R. S. Rahgavan, P. Raghavan, and J. M. Friedt, Phys. Rev. Lett. 30, 10 (1973).

23. E. J. Wilson, Ph.D. Thesis, Department of Chemistry, Carnegie-Mellon University, 1976 (unpublished).

24. Calculated using the tables in "Perturbed Angular Correlations", ed. by E. Karlsson, E. Matthias, and K. Seigbahn, North-Holland Publishing Co., Amsterdam, 1964.

25. F. A. Cotton and G. Wilkinson in "Advanced Inorganic Chemistry, A Comprehensive Text", Interscience Publishers, J. Wiley and Sons, 1962, p. 728.

26. J. G. White, Proc. Roy. Soc. London A266, 440 (1962).

27. T. Yamane and N. Davidson, Biochim. Biophys. Acta 55, 609 (1962).

28. F. X. Wilhelm and M. Duane, Biopolymers 8, 121 (1969).

29. T. Yamane and N. Davidson, Biochim. Biophys. Acta 55, 780 (1962).

30. T. Yamane and N. Davidson, J. Amer. Chem. Soc. 83, 2599 (1961).

31. J. H. Spencer, in "The Physics and Chemistry of DNA and RNA", W. B. Saunders Co., Philadelphia, 1972.

III. Heavy Ion Nuclear Reactions

A. Studies of Energetic Fragments from Heavy Ion Reactions Using a Counter Telescope with Element and Mass Resolution.

The objective of these experiments is to derive a detailed description of the reaction mechanism(s) leading to multinucleon exchange between heavy ions and medium mass targets at energies above 5 MeV/amu. In a systematic way, we plan to explore with light heavy ions those processes which have recently become of great importance in reactions involving very heavy ions.[1-3] The redistribution of mass and energy in nuclear collisions is being investigated in the system $^{65}Cu + ^{12}C$ using Si surface-barrier counter telescopes to obtain both Z and A identification on energetic reaction fragments from Li (Z = 3) through O (Z = 8). This type of experiment has been very successful at lower energies (i.e. tandem Van de Graaf accelerators) as a spectroscopic tool, but is relatively new in its application to higher energy heavy ion reactions and medium mass targets.

Initial experiments have been performed at the Yale Heavy Ion Accelerator prior to the shutdown of that facility. In that work, ^{65}Cu metal targets were bombarded with 126 MeV ^{12}C ions and boron, beryllium, and lithium reaction products were detected and measured with a counter telescope and particle identification system. Part of the incentive in that early investigation was the direct observation and cross-section measurement of ^{12}B fragments to compare with the unexpectedly large cross-section of the $^{65}Cu(^{12}C,X)^{65}Zn$ reaction determined by radioactivity methods.[4] If this latter reaction occurs via a two-body breakup, then the ^{65}Zn product corresponds to a phenomenological proton-neutron switching between projectile and target, or charge exchange mechanism, leading to ^{12}B as the complementary partner. The results of the Yale experiment were described in last year's Annual Report (COO-3246-15), and indicated that the cross-section for ^{12}B formation was not abnormally large,

but fitted rather well with the systematics of other light products observed in the same experiment.

During the current year we initiated an experimental collaboration with Dr. R. L. Ferguson, of Oak Ridge National Laboratory, for the purpose of pursuing and extending our investigations of heavy-ion reaction fragments at the Oak Ridge Isochronous Cyclotron. The experiments to date have continued with the $^{12}C + ^{65}Cu$ system at a bombarding energy of 130.7 MeV. Self-supporting targets of isotopically enriched ^{65}Cu metal foil were mounted in a large scattering chamber permanently located on an ORIC beam line. This particular experimental location has very good beam optics making it unnecessary to have mechanical beam collimators in the vicinity of the target area, and results in a significant reduction of extraneous background from slit scattering. Our first run used a ^{65}Cu target of thickness 3.40 mg/cm^2, and a counter telescope consisting of a 55.8 μm Si ΔE transmission detector backed by a stopping E detector of depletion depth 500 μm. The angular definition of the telescope was 0.1 msr, and corresponded to 0.7 deg. in the reaction plane. Signals from the two detectors were analyzed using a multiplexer-ADC system[5] coupled to an on-line computer. In this run the amplifier gains were set primarily for measurements of Be, B, and C fragments, and a survey was carried out at several angles with emphasis on very forward angles.

Our second run incorporated several significant improvements in the experiment. Since an abundance of ^{12}C beam intensity was available, we were able to use a much thinner ^{65}Cu metal target, of thickness 0.70 mg/cm^2. The E detector was replaced by one with a depletion depth of 1000 μm to stop energetic Li ions which had penetrated the original detector, and an anti-scatter mask was placed between the ΔE and E detectors. The ΔE transmission detector remained as 55.8 μm Si and the solid angle subtended by the counter telescope was kept

at approximately 0.1 msr. The amplifier gains were adjusted to encompass Li, Be, B, C, N, and O isotopes in the region of observation and differential cross-section data were obtained at angles from 5 deg to 35 deg.

An example of the experimental data from our counter telescope is shown in Fig. 10. This figure is a photograph of a composite computer output which displays the whole range of observation at full experimental resoltuion. The curved "streaks" in the ΔE vs. $(E-\Delta E)$ plane represent loci of identified reaction products whose intensity (number of events) at any point is quantitatively recorded in the third (perpendicular) dimension, and is roughly indicated by the density distribution of spots in the figure. The data in Fig. 10 were taken at a relatively forward angle, $\theta_{LAB} = 16°$, and it is apparent that the data are remarkably free of undesirable scattering, extraneous background, or other spurious events. The separation of adjacent elements by our telescope is quite large, and is indicated in Fig. 10 by the elemental symbols at the right of each band. Within each band of a given element, the several isotopes of that element are resolved and can be easily seen by visual inspection of Fig. 10. For example, the Be isotopes of mass numbers 7, 9, and 10 are displayed, with a rather prominent gap corresponding to the missing (particle unstable) ^{8}Be. Similarly, the B isotopes 10, 11, and 12, the C isotopes 11, 12, 13, and 14, and the N isotopes 13, 14, and 15 are distinct, and the O isotopes are separated although the numbers of these events are much smaller.

Fig. 11 presents a small section of the data from Fig. 10, as viewed from a graphics display oscilloscope coupled to the ORIC computer system. These data are the higher-energy half of the boron isotopes and the two-dimensional display matrix has been both compressed (x, y directions) and suppressed (z direction) in the computer to enhance the resolution for display purposes. A mask (the solid line) has been drawn on the display (Fig. 11) to isolate those events

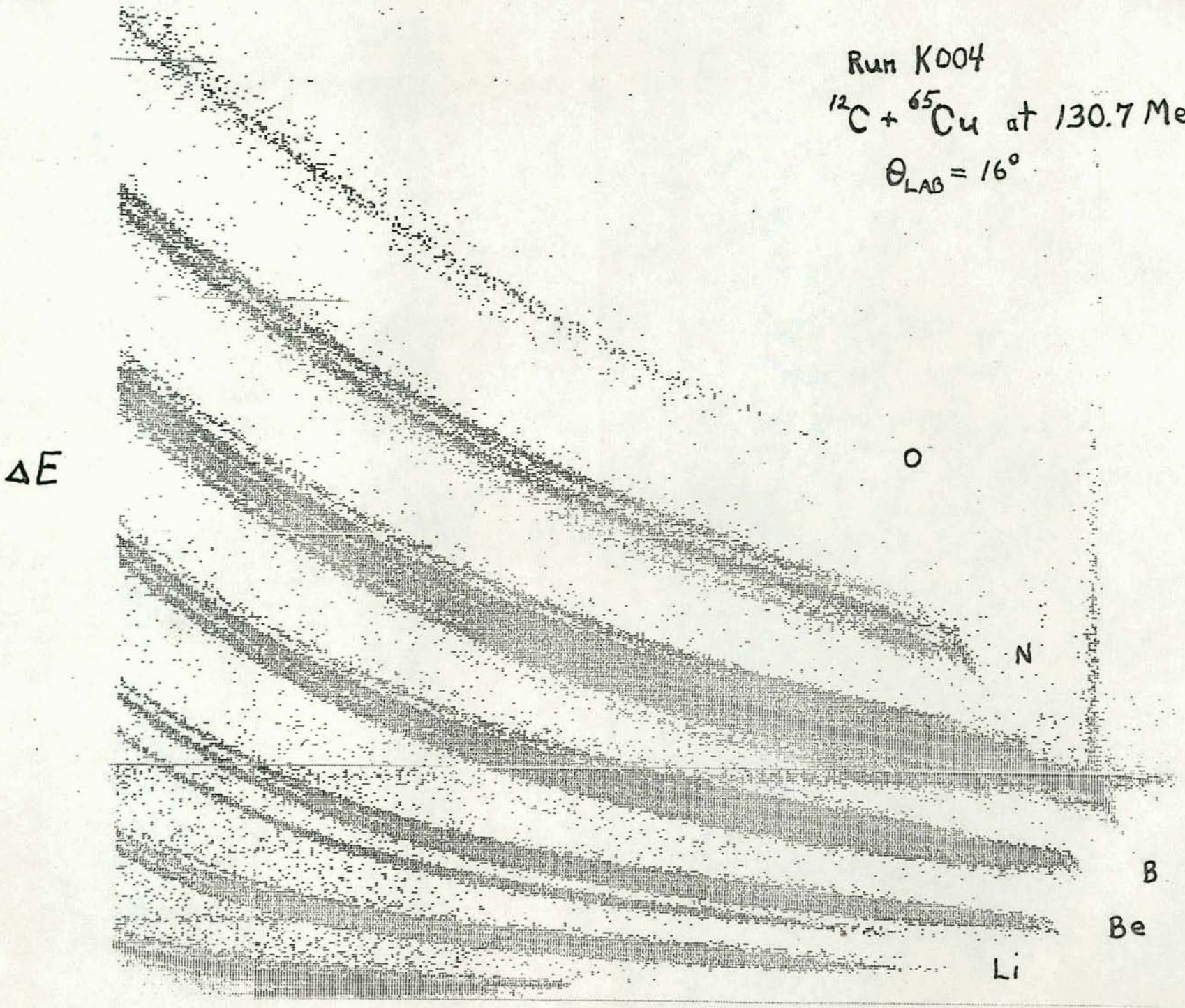

Figure 10.

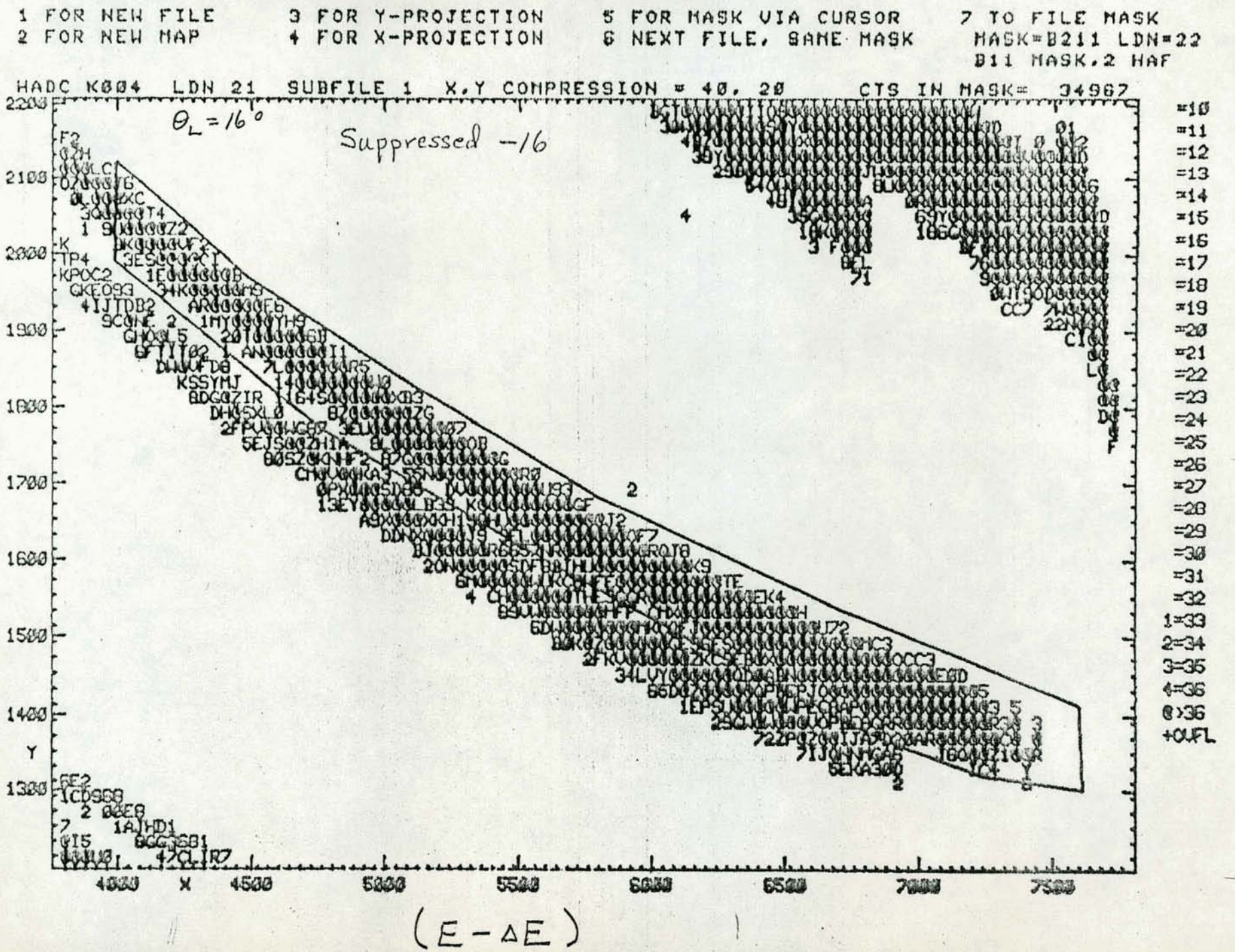
1 FOR NEW FILE
2 FOR NEW MAP
3 FOR Y-PROJECTION
4 FOR X-PROJECTION
5 FOR MASK VIA CURSOR
6 NEXT FILE, SAME MASK
7 TO FILE MASK
MASK=B211 LDN=22
B11 MASK.2 HAF
HADC K004 LDN 21 SUBFILE 1 X,Y COMPRESSION = 40, 20 CTS IN MASK= 34967
θL = 16°
Suppressed -16
ΔE
Y
X
(E - ΔE)
=10
=11
=12
=13
=14
=15
=16
=17
=18
=19
=20
=21
=22
=23
=24
=25
=26
=27
=28
=29
=30
=31
=32
1=33
2=34
3=35
4=36
@>36
+OVFL

Figure 11.

identified as ^{11}B fragments above a selected energy, and the sum of all events contained within the mask is proportional to the differential cross-section for ^{11}B production at the angle under consideration ($\theta_{LAB} = 16°$). The projection of the data within the mask onto the (E-ΔE) axis is shown in Fig. 12, and represents an approximate energy spectrum of the ^{11}B fragments selected for inspection. The detailed conversion to a true energy spectrum is a complicated process and has not yet been carried out in our preliminary analysis of the data. Except at low energies, the correction is relatively small and does not affect the spectral shape very much. The jagged nature of the energy spectrum in Fig. 12 is an artifact of the display program which connects adjacent data points by straight line segments. In this and succeeding figures of this type, the eye should draw a smooth curve through the statistical scatter of data to obtain a more realistic representation. The two large peaks in Fig. 12, however, are not display artifacts and exist in the data. They are found also in the ^{11}B spectra at other angles of observation, and exhibit a pronounced decrease in intensity with increasing angle. At the present time, their precise origin and significance is not understood but we consider them to be quite interesting and the subject of further study.

Figure 13 gives a repeat view (with increased suppression) of the data section containing boron isotopes. Here we have placed a mask around the ^{10}B events (upper half of the energy scale), and projected out the ^{10}B energy spectrum as shown in Fig. 14. It is quite clear even from this preliminary analysis that the ^{10}B energy spectrum is quite different from that of the ^{11}B fragments, and does not exhibit any peaks or structure above statistical fluctuations.

We have presented Figs. 10-14 as illustrations of the kind of data we have obtained in this experiment and the interactive processes of data manipulation

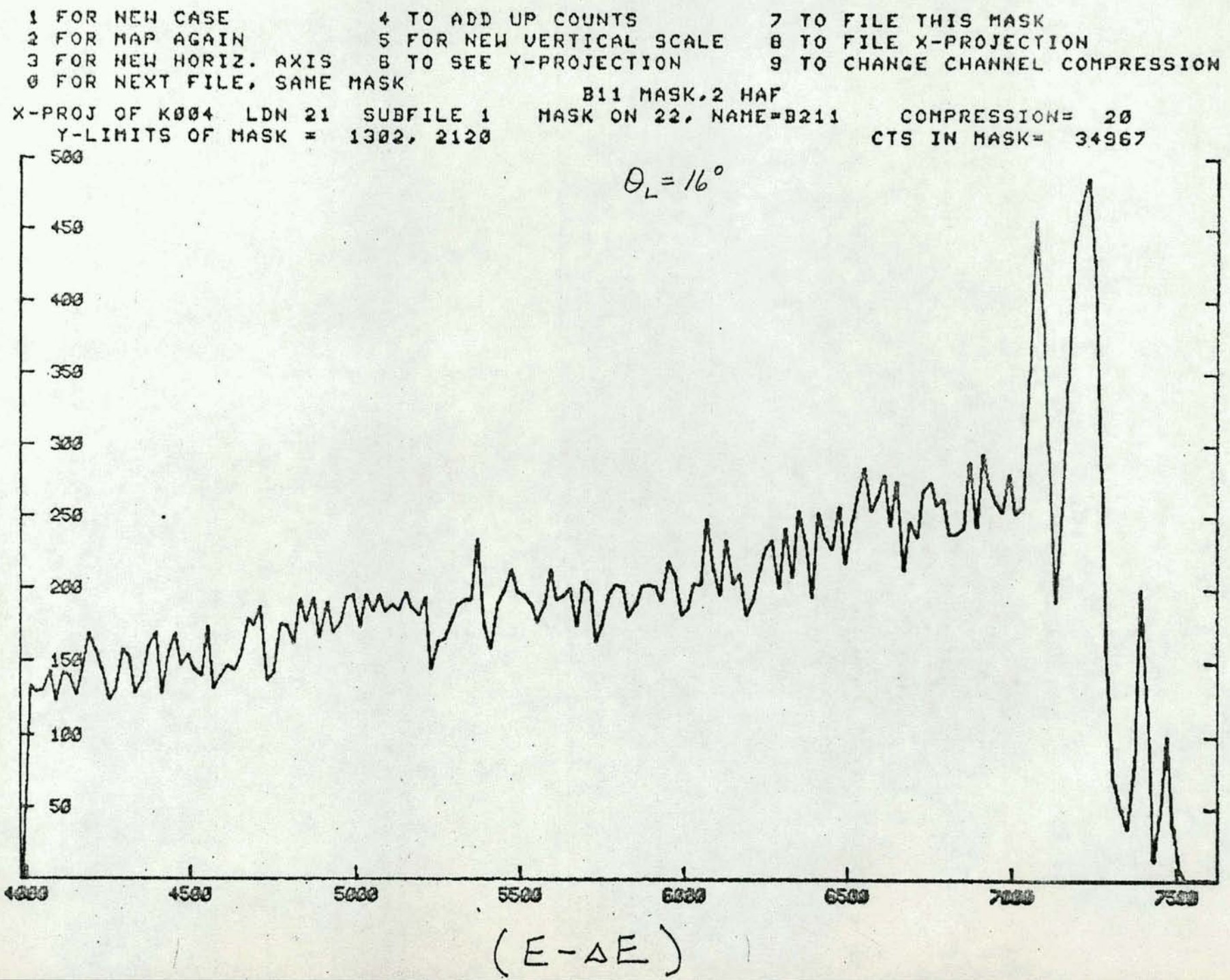
1 FOR NEW CASE
2 FOR MAP AGAIN
3 FOR NEW HORIZ. AXIS
0 FOR NEXT FILE, SAME MASK
4 TO ADD UP COUNTS
5 FOR NEW VERTICAL SCALE
8 TO SEE Y-PROJECTION
7 TO FILE THIS MASK
8 TO FILE X-PROJECTION
9 TO CHANGE CHANNEL COMPRESSION
B11 MASK,2 HAF
X-PROJ OF K004 LDN 21 SUBFILE 1 MASK ON 22, NAME=B211 COMPRESSION= 20
Y-LIMITS OF MASK = 1302, 2120 CTS IN MASK= 34967
θL = 16°
500
450
400
350
300
250
200
150
100
50
4000
4500
5000
5500
6000
6500
7000
7500
(E-ΔE)

Figure 12.

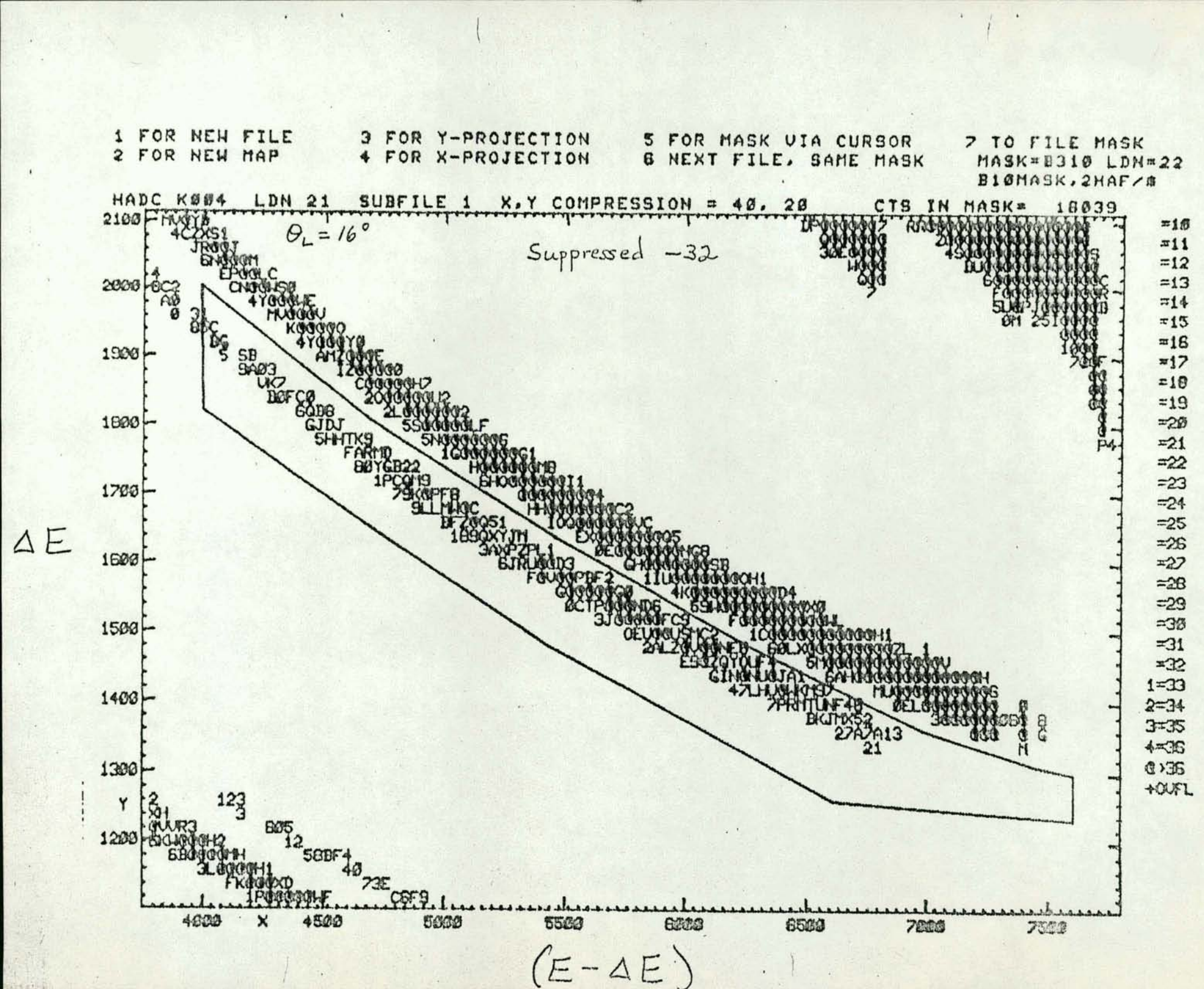
1 FOR NEW FILE
2 FOR NEW MAP
3 FOR Y-PROJECTION
4 FOR X-PROJECTION
5 FOR MASK VIA CURSOR
6 NEXT FILE, SAME MASK
7 TO FILE MASK
MASK=B310 LDN=22
B10MASK,2HAF/#
HADC K004 LDN 21 SUBFILE 1 X,Y COMPRESSION = 40, 20
CTS IN MASK= 18039
$\theta_L = 16°$
Suppressed -32
ΔE
(E-ΔE)
X
Y
4000
4500
5000
5500
6000
6500
7000
7500
1300
1400
1500
1600
1700
1800
1900
2000
2100
=10
=11
=12
=13
=14
=15
=16
=17
=18
=19
=20
=21
=22
=23
=24
=25
=26
=27
=28
=29
=30
=31
=32
1=33
2=34
3=35
4=35
@>36
+OVFL

Figure 13.

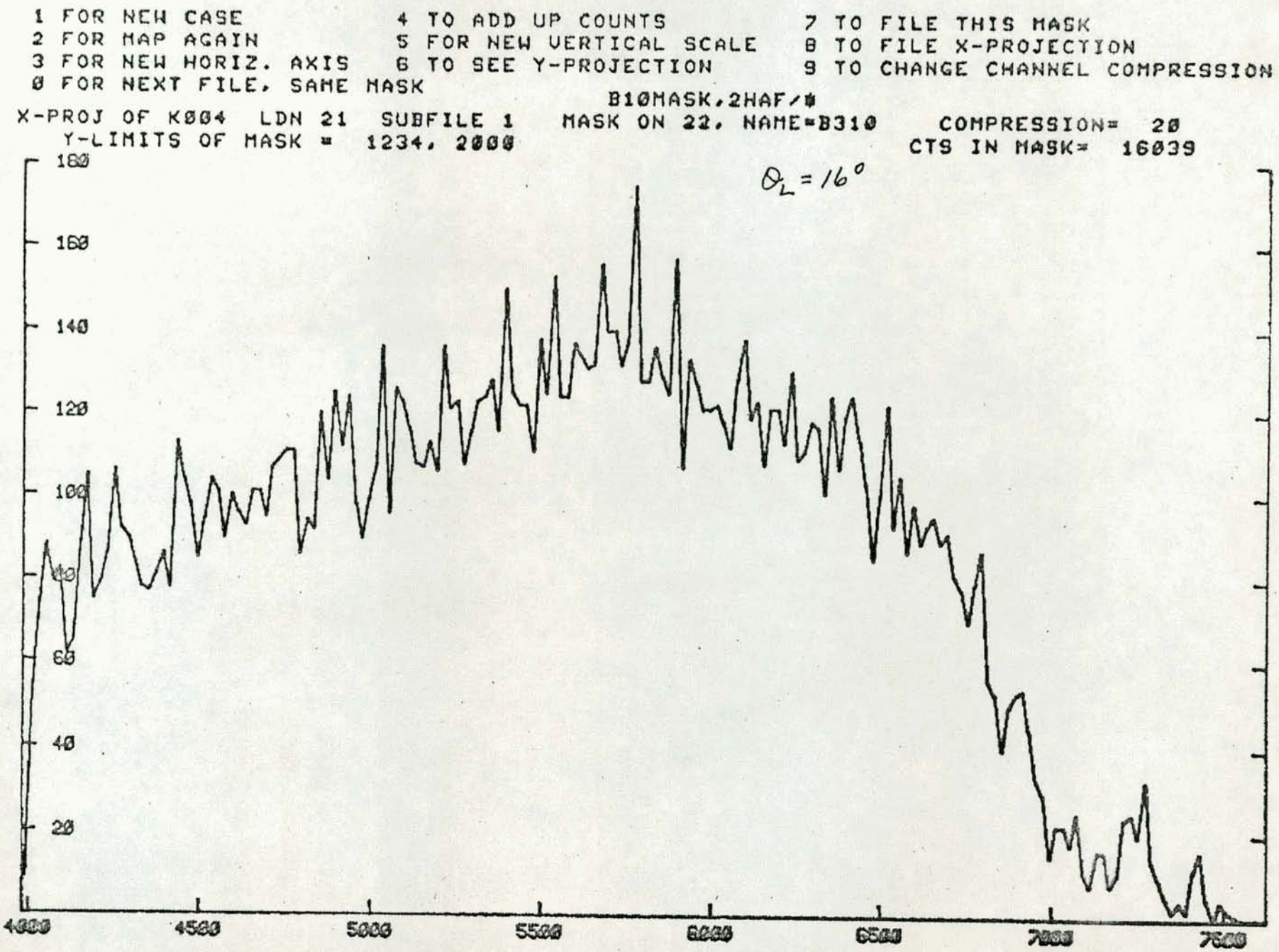
1 FOR NEW CASE
2 FOR MAP AGAIN
3 FOR NEW HORIZ. AXIS
0 FOR NEXT FILE, SAME MASK
4 TO ADD UP COUNTS
5 FOR NEW VERTICAL SCALE
6 TO SEE Y-PROJECTION
7 TO FILE THIS MASK
8 TO FILE X-PROJECTION
9 TO CHANGE CHANNEL COMPRESSION
B10MASK.2HAF/#
X-PROJ OF K004 LDN 21 SUBFILE 1 MASK ON 22. NAME=B310 COMPRESSION= 20
Y-LIMITS OF MASK = 1234. 2000
CTS IN MASK= 16039
θL = 16°
180
160
140
120
100
80
60
40
20
4000
4500
5000
5500
6000
6500
7000
7500
(E-ΔE)

Figure 14.

which are involved in extracting the energy spectra and differential cross-sections for individual elements and mass produced in the $^{12}C + ^{65}Cu$ reaction. It may be useful at this point to show a series of energy spectra obtained for different elements and isotopes, all corresponding to the same angle of observation. This has been done in Figs. 15-18 which give respectively the isotopic spectra of Li, Be, B, and N reaction products, all at $\theta_{LAB} = 22$ deg. In each case the full energy range observed for the elements in question is presented, but the energy scales are somewhat different in the several figures. Note also that the ordinate scale is indicated for each isotope and that these vary from one to another.

The Li and Be spectra in Figs. 15 and 16 respectively are relatively similar and demonstrate broad energy distributions which are distinctively different for the several isotopes of the same element. In general, the average energy increases with mass for a given Z (atomic number). The B spectra in Fig. 17 follow a similar trend for ^{10}B and ^{11}B isotopes, but the ^{12}B data seems to indicate a somewhat narrower energy distribution for this species. It is worth noting that the two peaks apparent in the ^{11}B spectra of Fig. 12 ($\theta_{LAB} = 16°$) are also visible in the ^{11}B data here, but at reduced intensity associated with the large angle ($\theta_{LAB} = 22°$). The N spectra in Fig. 18 seem to be somewhat different in character. The ^{13}N events are few in absolute number but are concentrated in a narrow region at the high energy end of the spectrum. It is tempting to speculate that this effect is a consequence of the lack of bound excited states in ^{13}N and hence only the ground state is observable. The ^{14}N and ^{15}N data seem to have a relative abundance of lower energy fragments.

At the present time the data analysis for this experiment is still in its preliminary stages and we are investigating several different sorting procedures with a view towards simplicity of manipulation.

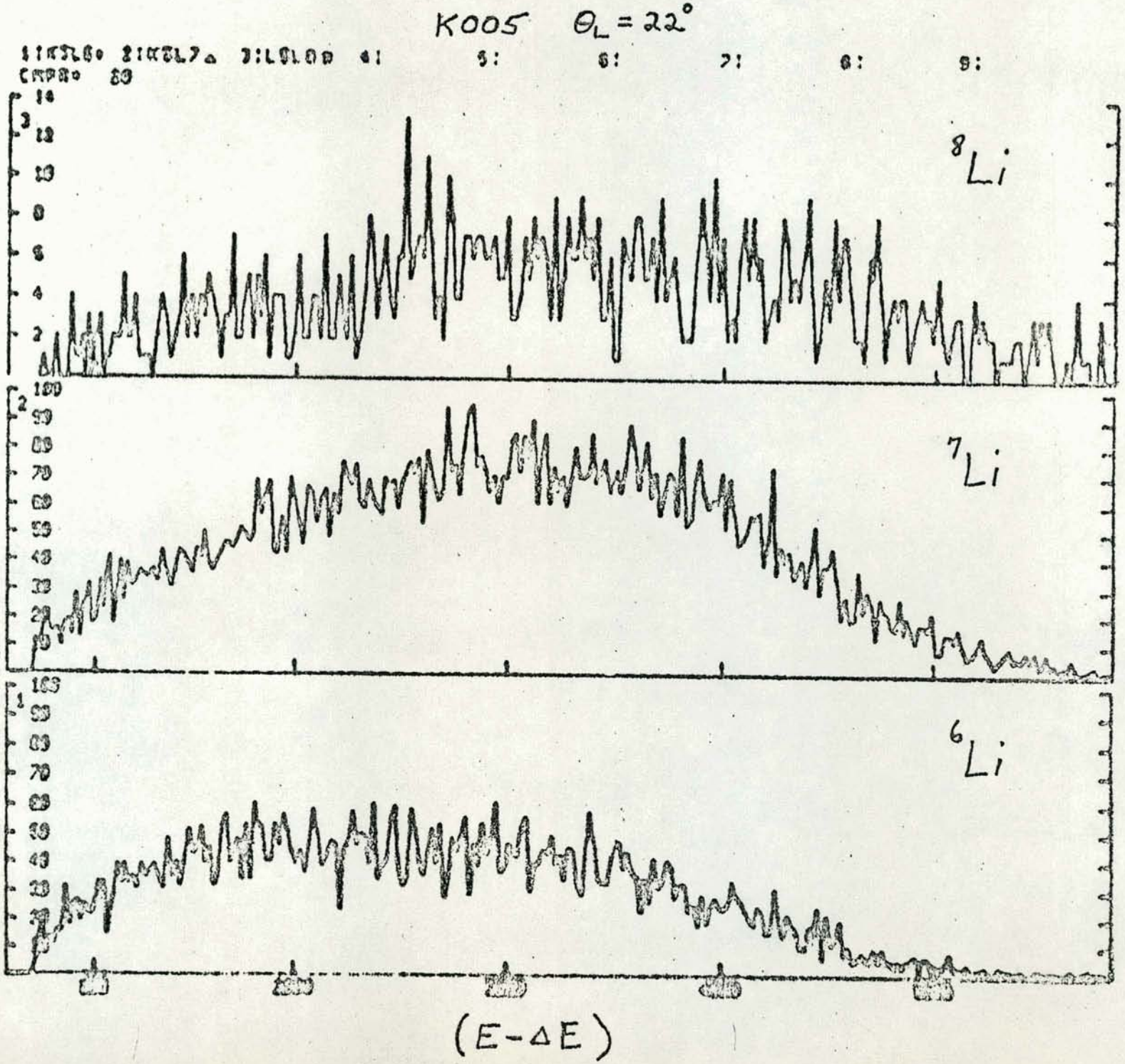

Figure 15.

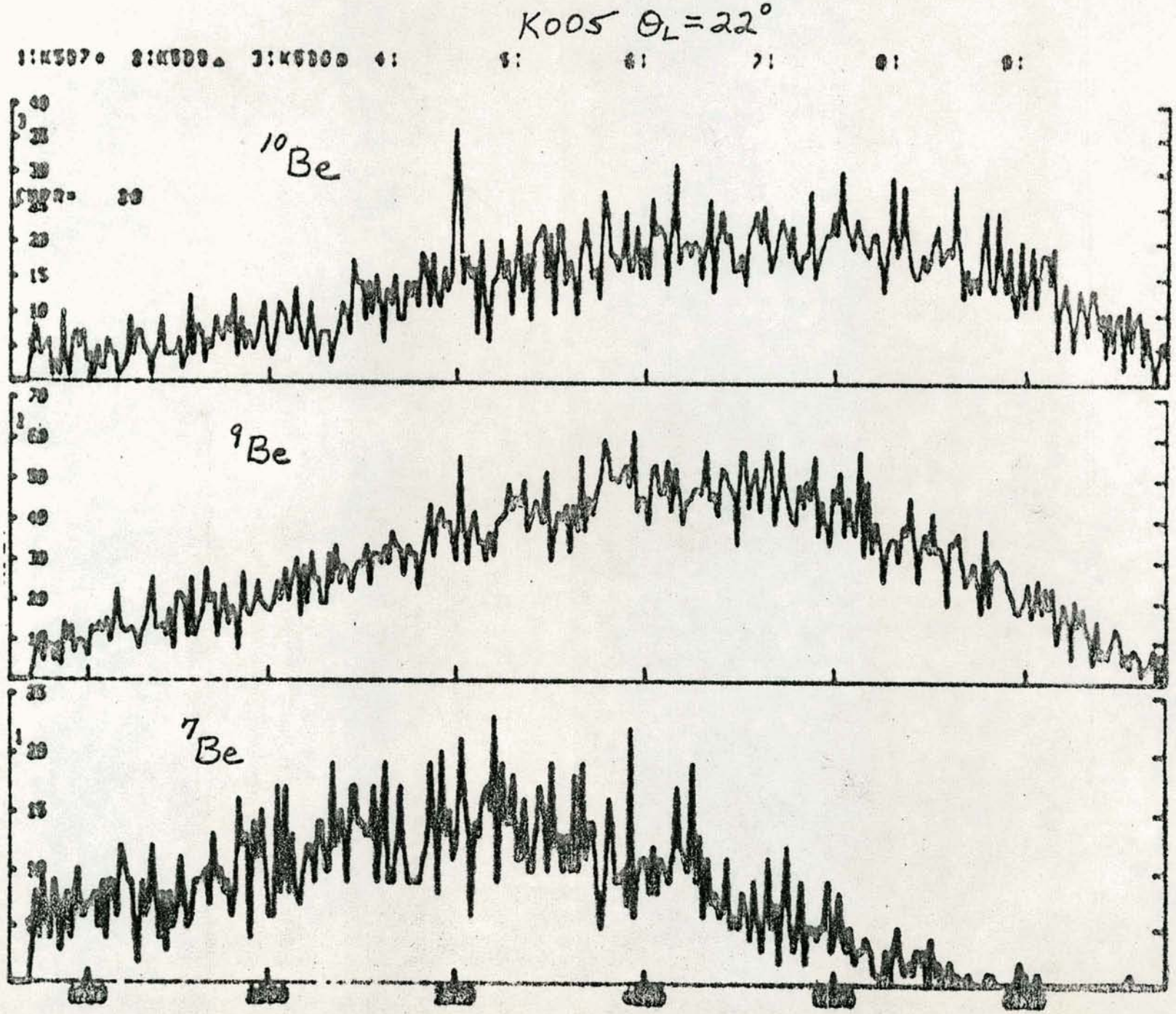

Figure 16.

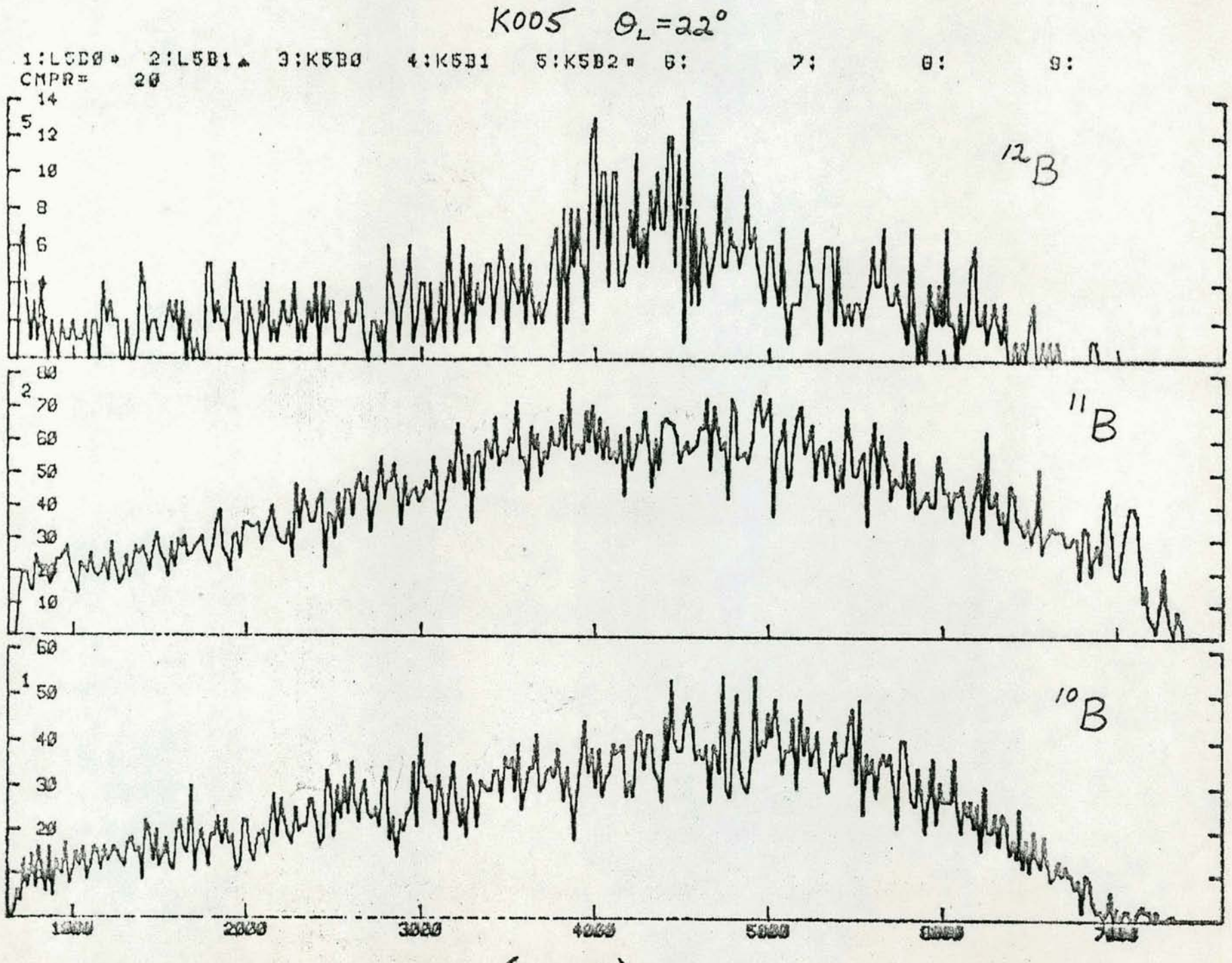
K005 $\theta_L = 22°$
1:LCD0 ▪ 2:L5B1 ▲ 3:K5B0 4:K5B1 5:K5B2 ▪ 6: 7: 8: 9:
CMPR= 20
^{12}B
^{11}B
^{10}B
(E−ΔE)

Figure 17.

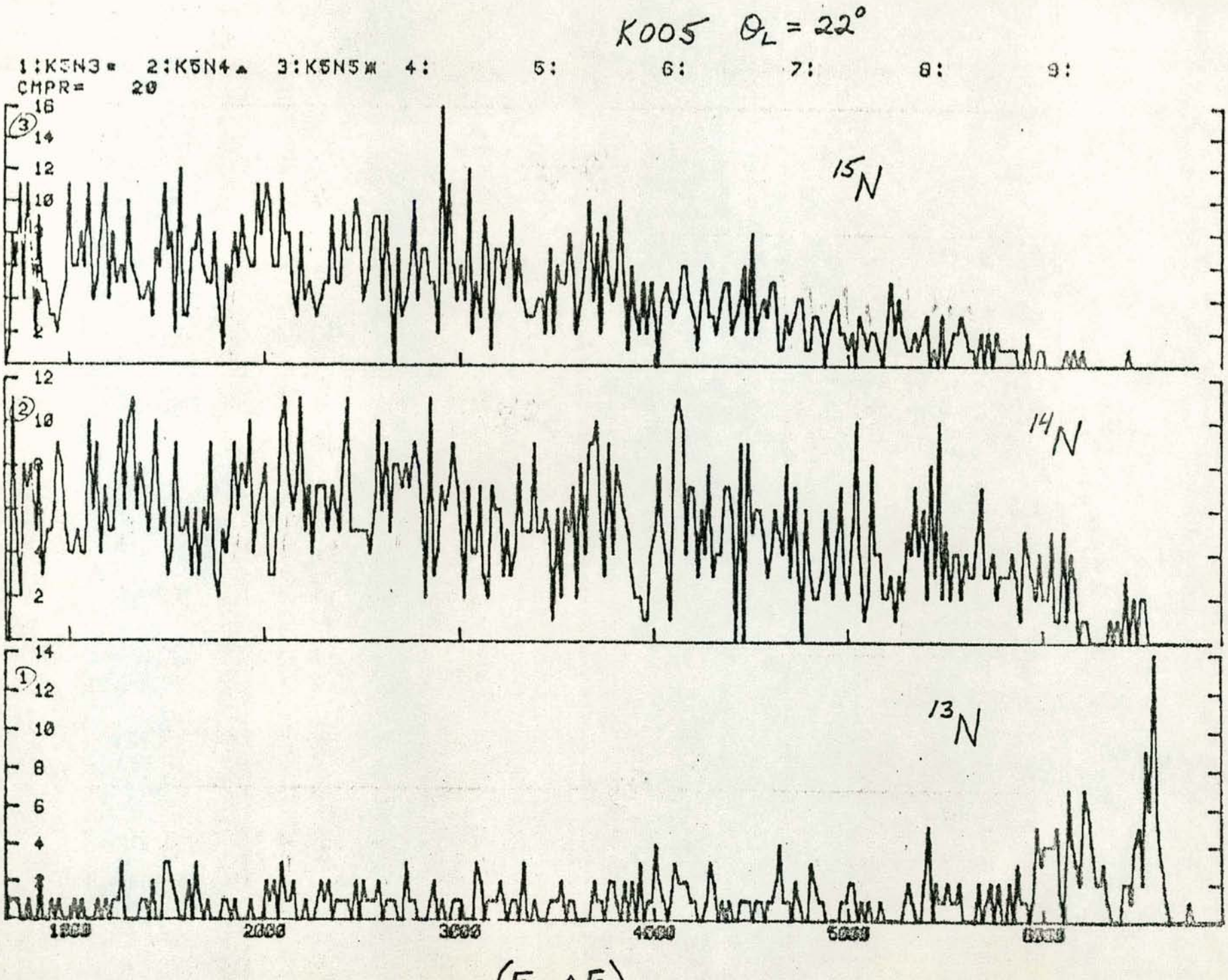
K005 $\theta_L = 22°$
1:K5N3 ▪ 2:K5N4 ▲ 3:K5N5 ✱ 4: 5: 6: 7: 8: 9:
CMPR= 20
^{15}N
^{14}N
^{13}N
(E-ΔE)

Figure 18.

B. Emission of Light Charged Particles in Hard Grazing Collisions of Very Heavy Ions.

An experimental program is well under way to investigate charged particle emission from highly excited fragments in collisions of heavy ions with complex nuclei. The research is carried out at the SuperHILAC accelerator of the Lawrence Berkeley Laboratory as a User Group collaboration with Professor J. M. Miller of Columbia University and Professor J. M. Alexander of SUNY at Stony Brook. The original concept was initiated by the Columbia-Stony Brook team, and during the past year a recognition of considerable overlap in interests and plans has resulted in the incorporation of our Carnegie-Mellon group to form a three-university collaboration.

It is by now well known[6] that the reactions between complex nuclei of very high Z_1Z_2 product (e.g. $^{197}Au + ^{86}Kr$) are dominated by deep inelastic (or quasifission) processes. For somewhat smaller Z_1Z_2 products (e.g. $^{197}Au + ^{40}Ar$) most reaction channels seem to be similar to nuclear fission that has been characterized for some time with light heavy ion projectiles (He-Ne). At still smaller Z_1Z_2 products (e.g. $^{136}Ba + ^{20}Ne$ or $^{60}Ni + ^{86}Kr$) complete fusion and evaporation processes are very important. We are studying the emission of H and He products in some of the above reactions with the objective of characterizing the emission mechanisms and hence gaining insight into the properties of the emitters.

Most of our work at the SuperHILAC has been devoted to reactions of 725-MeV ^{86}Kr with ^{197}Au. The experiments were performed using a three-element solid-state counter telescope consisting of a 45 μm Si surface-barrier ΔE_1 detector, a 500 μm Si surface-barrier ΔE_2 detector, and a 5000 μm Si(Li) E_3 detector. This design of detection system yielded good separations and unambiguous identification of ^{1}H, ^{2}H, ^{3}H, ^{3}He, and ^{4}He over a wide dynamic

range. Signals from the three detectors as well as from monitor counters were digitized in a multiplexed ADC system and recorded event-by-event on magnetic tape, as well as being analyzed on-line by a computer system for display purposes. The first experiments carried out were "singles" experiments with the counter telescope, in which energy spectra of H and He fragments have been measured at several angles from 10° to 145°. The results obtained for the proton spectra from $^{86}Kr + ^{197}Au$ are shown in Fig. 19. The ordinate is plotted as the double differential cross section in absolute units of (mb/sr-MeV). Similar data for deuterons and tritons are indicated in Fig. 20, and the corresponding results for alpha particles are presented in Fig. 21.

The energy and angular distributions of the light particles from the reactions of ^{86}Kr with ^{197}Au are, on the whole, consistent with the hypothesis that they are emitted in the equilibrium de-excitation of the excited transfer products formed in these reactions. The consequences of this idea are being investigated by means of a Monte Carlo calculation, using as input data (1) the energy and angular distributions of the transfer products in the Kr + Pb reactions as reported by Vandenbosch, et al.,[7] and (2) the energy spectra in the equilibrium emission of light particles from Kr-like and Au-like excited transfer products as estimated from a combination of theory and experimental results for excited nuclides similar to those under study here. We hope to be able to derive the probabilities for emission of the various light particles from the separated Au-like and Kr-like transfer reaction products.

In order to provide experimental data on the relationships of the emitted light particles to the transfer reaction partners, we have proposed and now carried out a coincidence and correlation experiment in which we have measured the energy spectra of light particles (H and He) emitted at selected

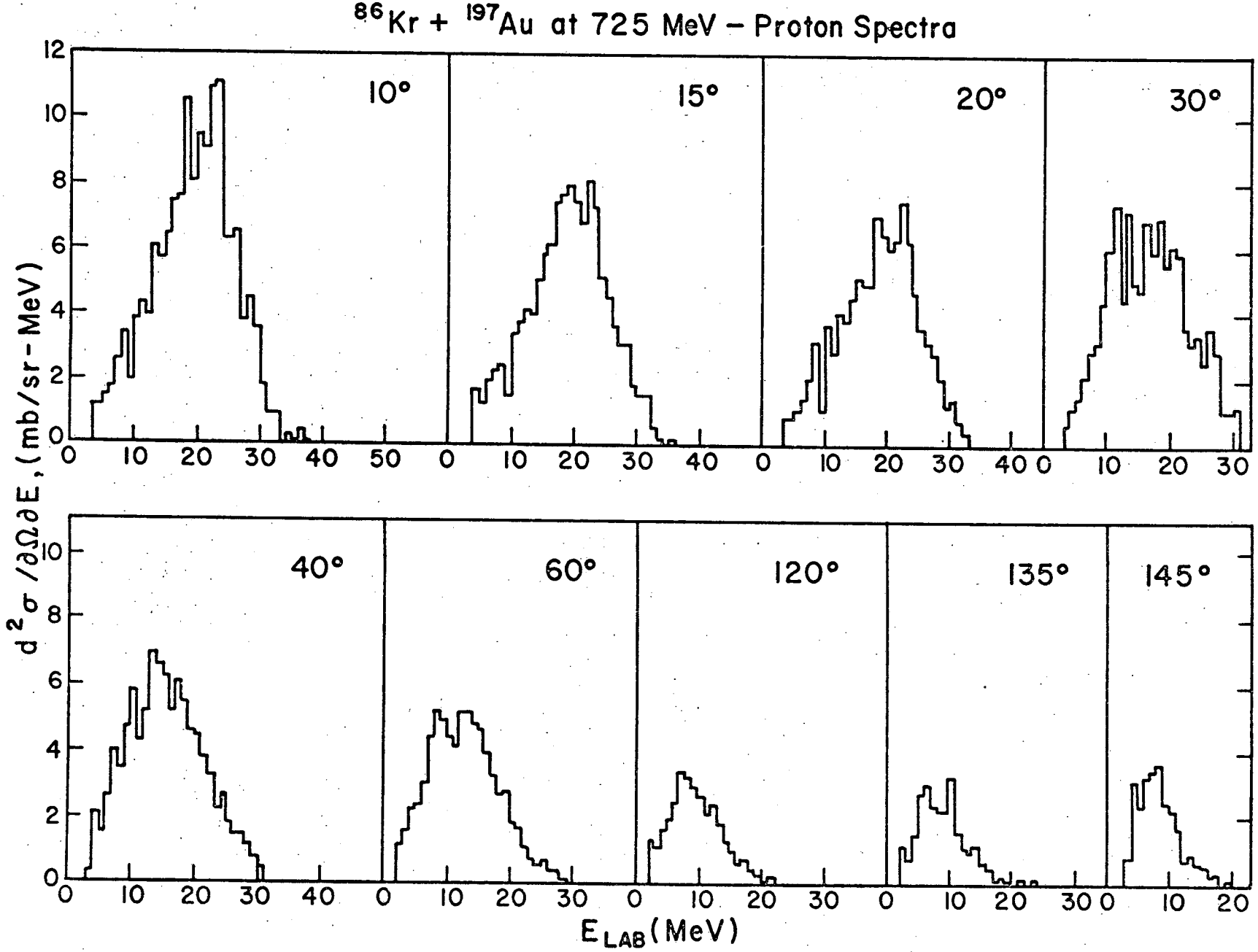
$^{86}Kr + ^{197}Au$ at 725 MeV – Proton Spectra
10°
15°
20°
30°
40°
60°
120°
135°
145°
$d^2\sigma/\partial\Omega\partial E$, (mb/sr-MeV)
E_{LAB} (MeV)

Figure 19.

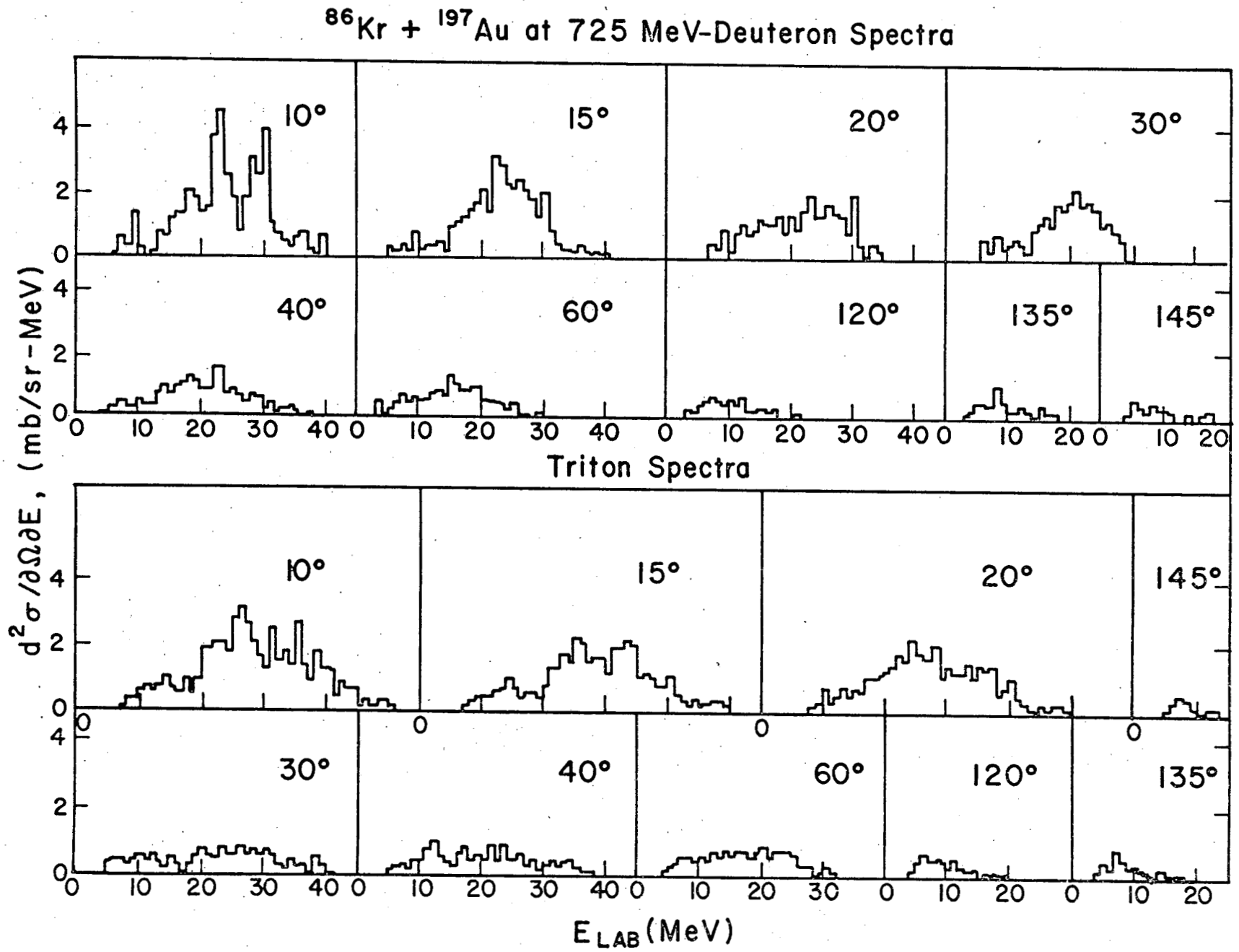
^{86}Kr + ^{197}Au at 725 MeV-Deuteron Spectra
10°
15°
20°
30°
40°
60°
120°
135°
145°
Triton Spectra
$d^2\sigma/d\Omega dE$, (mb/sr-MeV)
E_{LAB} (MeV)

Figure 20.

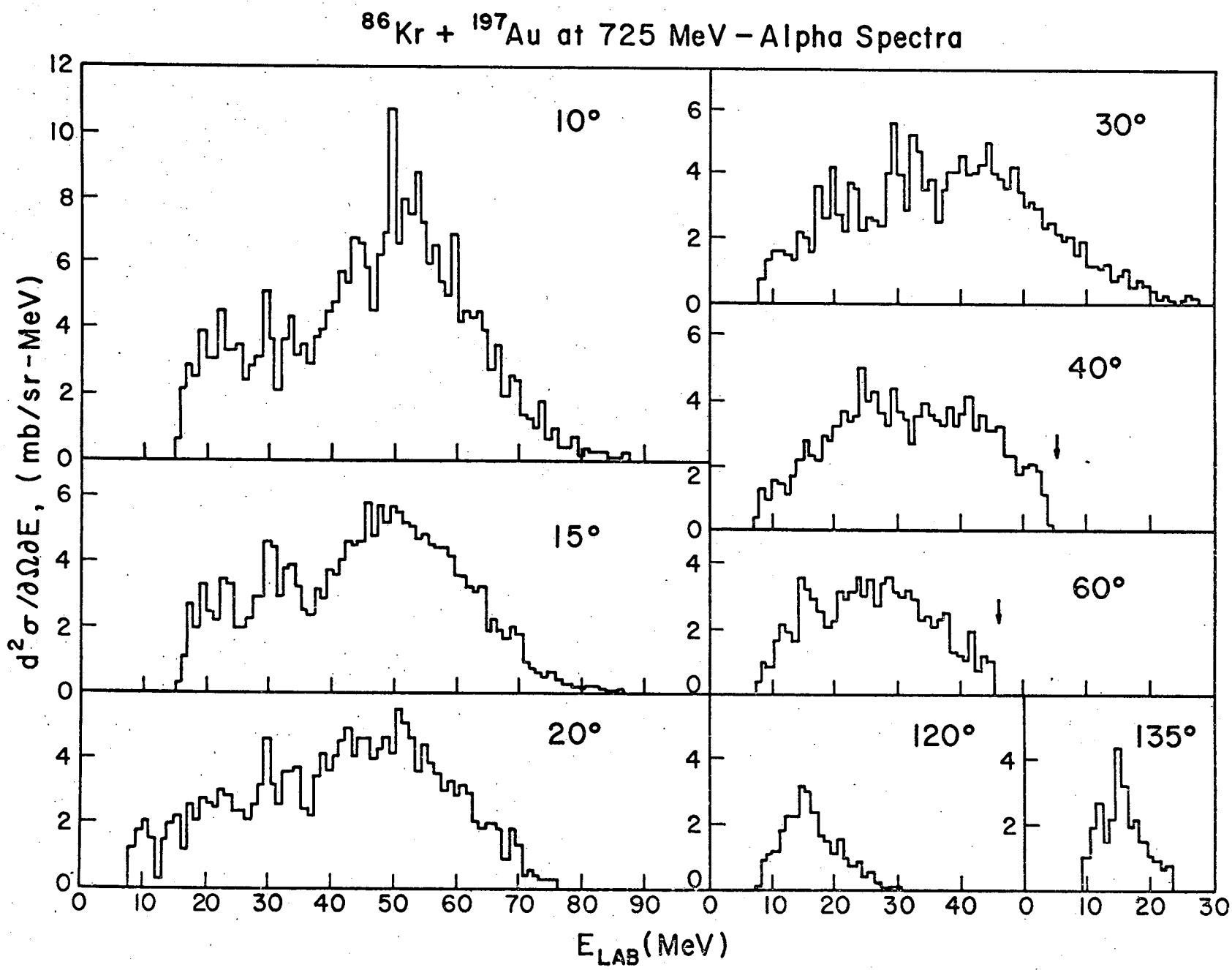
86Kr + 197Au at 725 MeV – Alpha Spectra
10°
15°
20°
30°
40°
60°
120°
135°
d²σ/dΩdE, (mb/sr-MeV)
E_LAB (MeV)

Figure 21.

angles in coincidence with Kr (or Au) detected at a particular angle following a deeply inelastic scattering process from 725-MeV ^{86}Kr on ^{197}Au. By careful consideration of the kinematics associated with the deep inelastic events, it is possible to arrange the various detectors at angles which emphasize or exclude the detection of light particles from a particular fragment and this additional feature is a significant advantage in the interpretation of the data. The value of the coincidence experiment lies in the capability of its yielding precise information on the channel momentum corresponding to a given light-particle emission, thereby providing a more stringent test for the hypothesis that most, if not all, of the observed light-charged-particles are emitted from equilibrated reaction products. Furthermore, the relative yields of H and He emitted from transfer fragments with known momenta, excitation energy, and approximate identity can provide information on the angular momenta associated with these fragments, which is, of course, of considerable importance to any theoretical understanding of the deep inelastic process. In addition, while the experiments so far suggest that nearly all of the light particles are emitted from essentially equilibrated and separated reaction products, it is not unreasonable to expect that there may be emission from the composite system as, for example, alpha emission from the "neck" in fission. In the system $^{86}Kr + ^{197}Au$, the neck between the fragments may be quite hot and if particles are emitted from this region, the best hope for distinguishing them is by their angular distribution with respect to the "scission" axis. This also was one of the objectives of the coincidence experiment.

The experiment was carried out at the SuperHILAC in the new 30" scattering chamber in the Users Area. The Kr-like or Au-like fragments (as well as fission fragments) were detected in a gas-telescope consisting of a thin-window gas ionization chamber as a ΔE counter and a 500 μm Si surface barrier

detector as the stopping counter E_5. A large-angle 3-detector solid-state telescope of the type described above was used to identify the H and He products. As we have already measured the singles angular distributions with good angular resolution, the present set-up was designed to emphasize the ratio of coincident to singles events with much larger angles of acceptance. The gas telescope subtended a solid angle of approximately 1.4 msr and the solid-state telescope covered about 20 msr. In addition to the usual logic and coincidence requirements imposed on the two detector telescopes, an acceptable event in the light-particle telescope started a time-to-amplitude converter (TAC) which was subsequently stopped by the arrival of a heavy fragment in the gas telescope. This time information served not only as a coincidence device but also provided crude time-of-flight data which was useful in distinguishing Kr fragments from Au fragments on-line. In this experiment we used the new Mod Comp IV computer as the primary data acquisition system with great success. In addition to having visual displays of the singles spectra in each of the detectors and the TAC, we were also able to observe 2-dimensional ΔE-E displays from both the solid-state and gas telescopes and each of them displayed as a function of the TAC output.

Throughout this run, the accelerator, the computer, and all of our instrumentation performed with minimum difficulty and we were able to accomplish the full objective of the experiment, at least so far as data-taking is concerned. As the experiment was quite recent, none of the data has yet been analyzed other than for consistency checks, and hence we are unable to report specific results at the present time.

C. Fusion, Fission, and Charged Particle Emission from ^{194}Hg Compound Nuclei.

A strong advantage that heavy-ion beams provide for nuclear reactions studies is the opportunity to separate the effects of angular momentum from

those of energy. The separation is not simple, however, and cannot be made directly. One must combine the results obtained from theory and well-chosen experiments. The difficulty is that one cannot control the impact parameter (or ℓ value) of each reaction channel as we can control the energy and mass of the collision partners. Thus we must try to calibrate our theoretical calculations by obtaining systematic experimental information as a function of angular momentum (ℓ) and energy (E), from reactions of known mechanisms. Then we may use the observed reaction characteristics along with our theories to infer ℓ and E deposition for reactions of unknown mechanism (i.e. deep inelastic scattering).

In a collaboration between Carnegie-Mellon, Columbia, and Stony Brook, we have been carrying out experiments at the 88" Cyclotron of the Lawrence Berkeley Laboratory to provide systematic data from heavy-ion reactions of known mechanism. In particular, we are using compound nucleus reaction processes to calibrate the characteristics of fission and H and He emission from equilibrated intermediate nuclei. The techniques employed are very similar to those described in Section IIIB above for the SuperHILAC experiments, namely solid-state telescopes for light-charged particle identification and a gas ionization chamber telescope for heavy fragment detection. We have measured the energy and angular distributions (and consequently the cross-sections) for H, He, and fission fragments, as well as for the evaporation residues from full-momentum-transfer processes. The reactions under investigation are:

$$121.0\text{-MeV } {}^{12}C + {}^{182}W \rightarrow {}^{194}Hg^{*} \quad (E^{*} = 97.5\text{-MeV})$$

$$135.2\text{-MeV } {}^{19}F + {}^{175}Lu \rightarrow {}^{194}Hg^{*} \quad (E^{*} = 97.5\text{-MeV})$$

The maximum angular momenta in the entrance channels of these two reactions can be calculated from the systematics of strong interaction radii, and are 66 $\hbar$ and

75 $\hbar$ respectively. The proximity of ^{194}Hg to ^{197}Au allows these experiments to have a direct bearing on our ^{86}Kr + ^{197}Au studies at the SuperHILAC, and it is fortunate that the 88" cyclotron can produce matched ^{12}C and ^{19}F beams to yield ^{194}Hg* at the same excitation energy but with differing angular momentum distributions.

Fig. 22 presents a logarithmic plot of the angular distribtions for evaporation residues from the two reactions studied. The strong forward-peaking and the confinement of the evaporation residues to small angles are features expected here for collisions involving total momentum transfer. The difference in slopes fro the two reactions in Fig. 22 arises from the different velocities of the center-of-mass in the ^{12}C and ^{19}F induced reactions.

Our measurements of the fission-fragment angular distributions are shown in Fig. 23. These distributions for both the ^{12}C and ^{19}F reactions are found to be proportional to $(\sin \theta_{c.m.})^{-1}$, which would be predicted for fission following compound-nucleus formation.

Some representative charged particle spectra (singles) for the ^{12}C + ^{182}W and ^{19}F + ^{175}Lu reactions are presented in Fig. 24. The upper part of the figure gives ^{4}He energy spectra at a forward angle and at two backward angles for the ^{19}F induced reactions. The lower part of Fig. 24 compares proton energy spectra at a backward angle for the two heavy-ion reactions leading to ^{194}Hg at an excitation energy E^* = 97.5-MeV. The H and He spectra at other angles are similar and vary in a manner consistent with that indicated in Fig. 24. The angular distribution of ^{4}He from the ^{19}F + ^{175}Lu reactions is plotted on a logarithmic scale in Fig. 25. This figure demonstrates very nicely that the alpha-particle emission probability is enhanced in the forward direction but becomes quite flat at angles in the backward hemisphere. In fact, we have observed that the angular distributions of H and He for both the ^{12}C and ^{19}F

Figure 22.

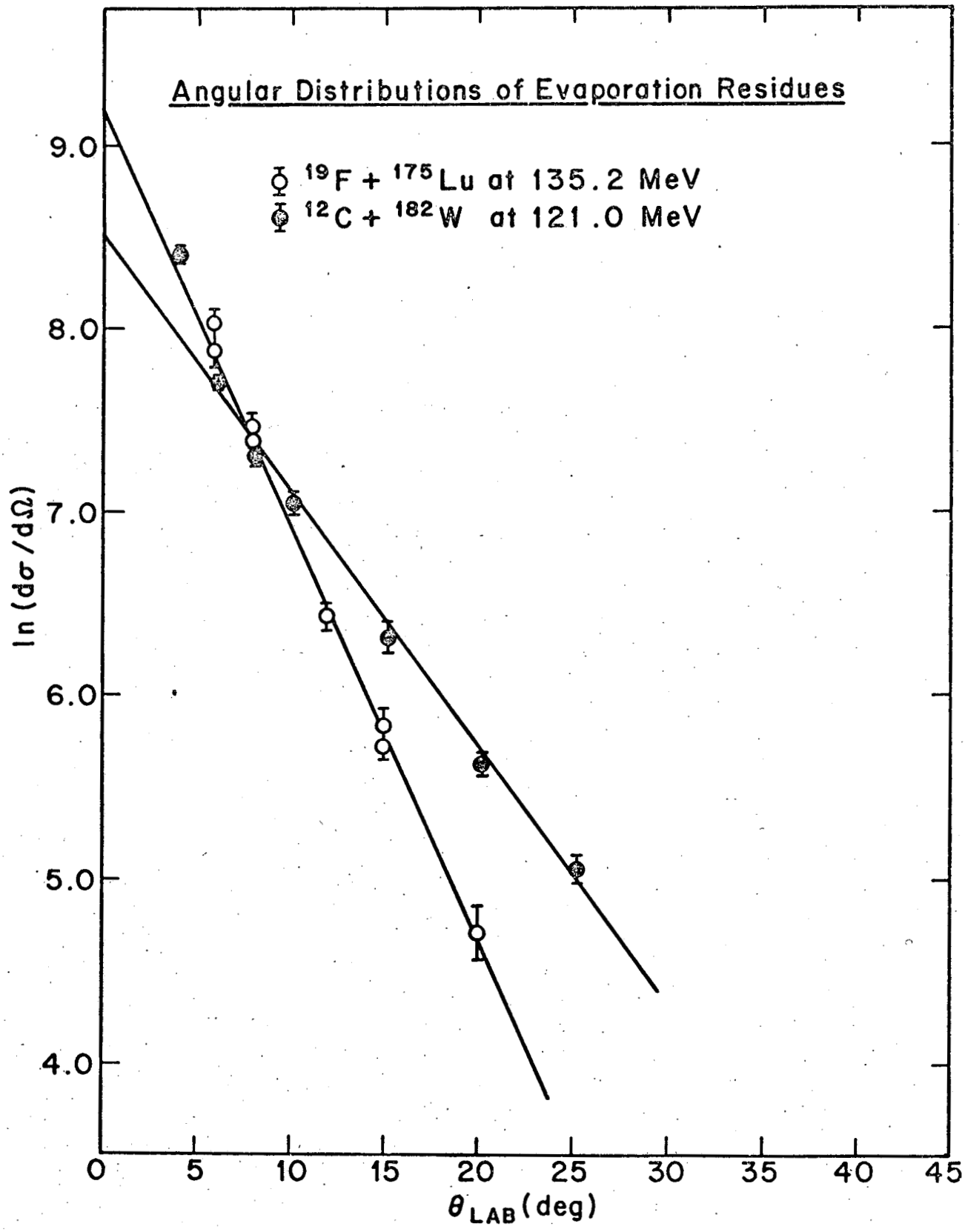
Angular Distributions of Evaporation Residues
$^{19}F + ^{175}Lu$ at 135.2 MeV
$^{12}C + ^{182}W$ at 121.0 MeV
ln (dσ/dΩ)
9.0
8.0
7.0
6.0
5.0
4.0
0
5
10
15
20
25
30
35
40
45
θ_{LAB} (deg)

Figure 23.

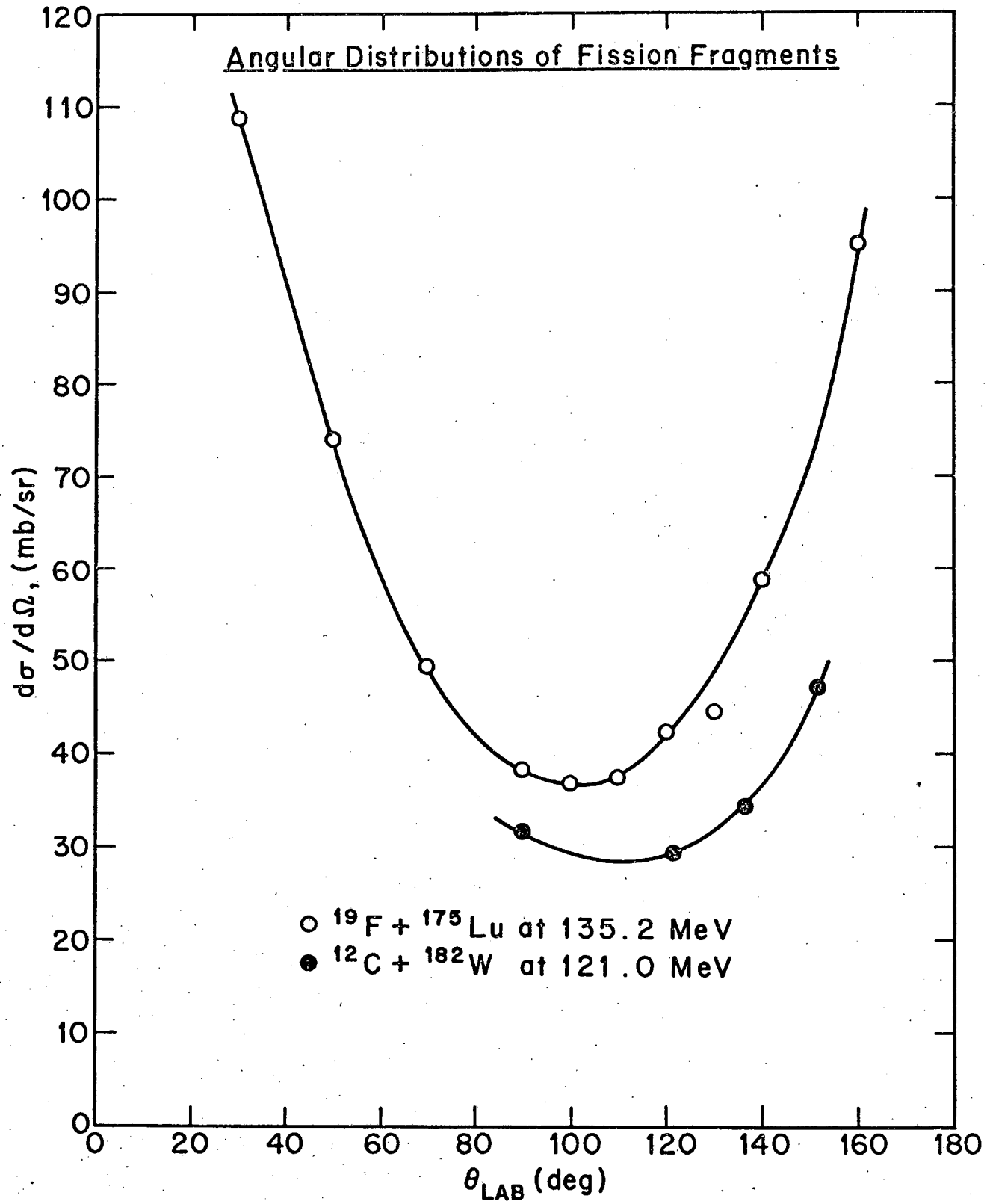
Angular Distributions of Fission Fragments
dσ/dΩ, (mb/sr)
θLAB (deg)
○ 19F + 175Lu at 135.2 MeV
● 12C + 182W at 121.0 MeV
0
10
20
30
40
50
60
70
80
90
100
110
120
0
20
40
60
80
100
120
140
160
180

Figure 24.

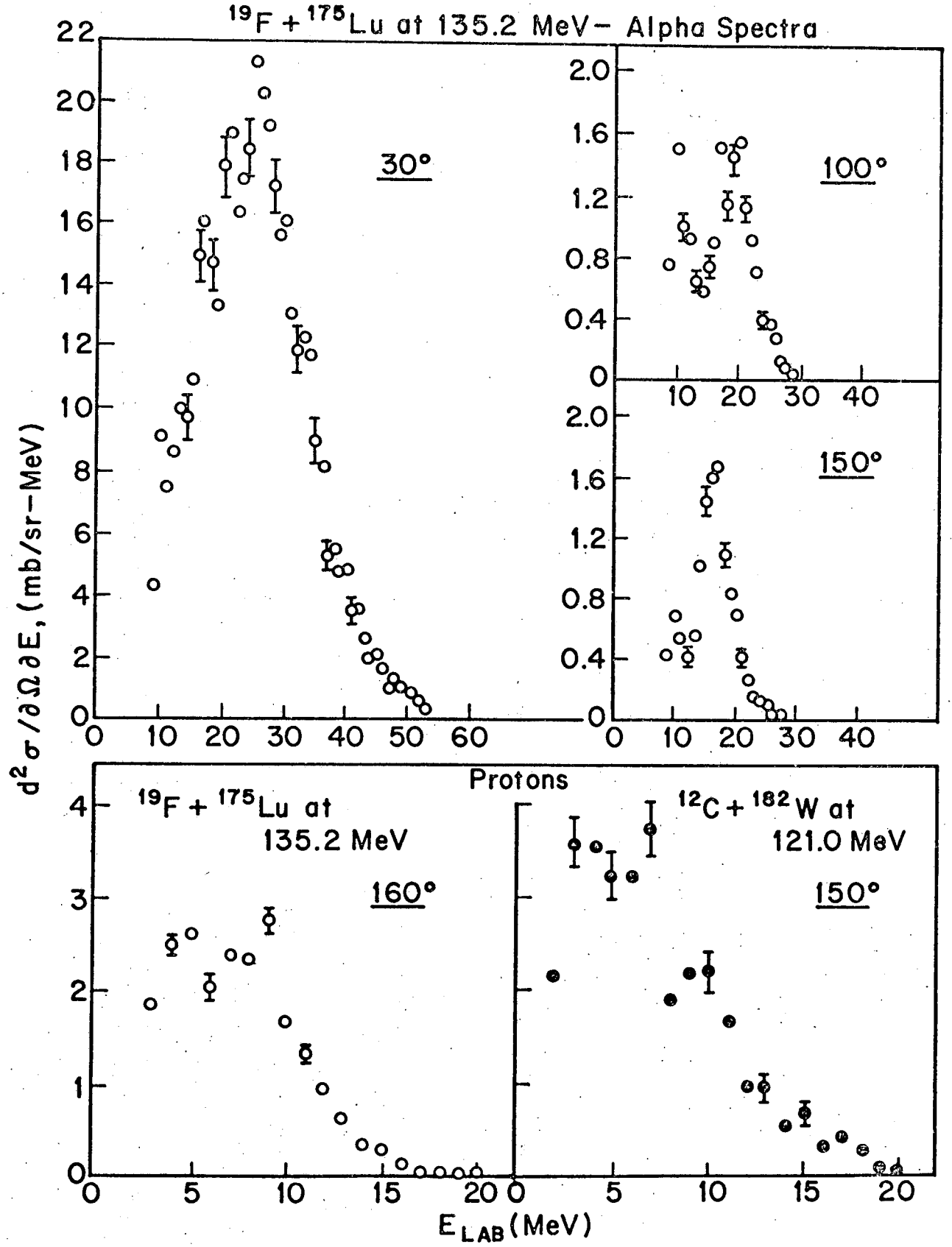
$^{19}F + ^{175}Lu$ at 135.2 MeV– Alpha Spectra
30°
100°
150°
$d^2\sigma/\partial\Omega\partial E$, (mb/sr–MeV)
Protons
$^{19}F + ^{175}Lu$ at 135.2 MeV
160°
$^{12}C + ^{182}W$ at 121.0 MeV
150°
E_{LAB} (MeV)

Figure 25.

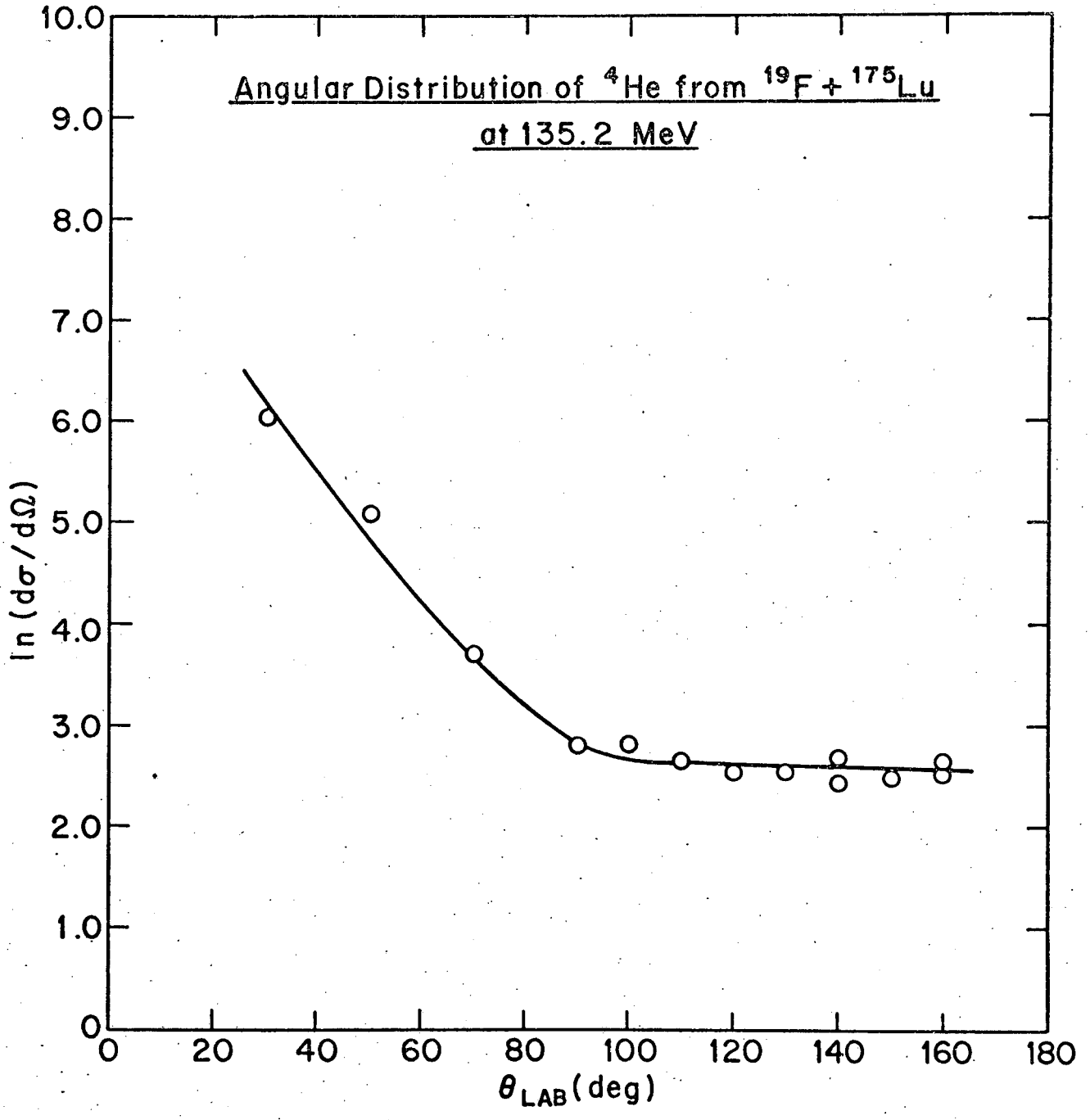
Angular Distribution of ^{4}He from $^{19}F + ^{175}Lu$
at 135.2 MeV
10.0
9.0
8.0
7.0
6.0
5.0
4.0
3.0
2.0
1.0
0
ln(dσ/dΩ)
0
20
40
60
80
100
120
140
160
180
θ_{LAB}(deg)

induced reactions are essentially isotropic aft of 90° c.m. The c.m. energy distributions of ^{1}H and ^{4}He products (aft of 90° c.m.) are also independent of angle. These observations provide classic signatures of particle evaporation from an equilibrated composite system.

In Table VA we present preliminary values of the cross-sections for evaporation residues, fission, and the isotropic (compound-nucleus) components of H and He emission.

Table VA. Integrated Cross-Sections (mb) for Products (only the compound nucleus components) from Several Heavy Ion Reactions.

Product \ Reaction	$^{12}C + ^{182}W$ 121-MeV (lab)	$^{19}F + ^{175}Lu$ 135-MeV (lab)	$^{20}Ne + ^{197}Au$ 170-MeV (lab)
H	400	276	75 - 300
He	142	182 ± 80	126
Fission	512 ± 50	756 ± 76	1400
Evap. residues	450 ± 100	361 ± 80	-

For comparative purposes, we have also included in the table some approximate cross sections for the $^{20}Ne + ^{197}Au$ system. (These rough numbers were obtained at the SuperHILAC during a "tune-up" run when the Kr beam was unattainable.) We emphasize that these results are based only on a preliminary analysis of the data and may change somewhat with refinement. Table VB contains the derived angular momentum cut-off values that divide up the entrance channel spectrum of ℓ-waves into various "reaction zones", as computed with the standard sharp cut-off approximations. We take the sum of the cross sections for fission plus evaporation residues to represent the cross-section for all equilibrated composite nuclei. It can be seen from Table VB that there is significant

Table VB. Derived Angular Momentum Cut-Offs ($\hbar$) for Several Heavy Ion Reactions

Channel \ Reaction	$^{12}C + ^{182}W$ 121-MeV (lab)	$^{19}F + ^{175}Lu$ 135-MeV (lab)
Evap. residues only	29 ± 3	33 ± 4
Evap. residues plus fission	42 ± 3	59 ± 3
Maximum ℓ (calculated for all channels)	66	75

competition involving non-equilibrium reaction channels and that this competition clearly depends on the incident (entrance) reaction channels.

At the present time, the experimental data are being analyzed in terms of the influence of angular momentum slices in the entrance channel on the decay probabilities in the various exit channels.[8] These results should provide a useful comparison with theory. The liquid drop and statistical models say with great confidence that fission probability increases rapidly with ℓ for ^{194}Hg. The statistical model says (with much less certainty) that ^{4}He emission probability decreases with ℓ for ^{194}Hg. We hope our results can indicate the important decay signatures for ^{194}Hg at 97.5-MeV; i.e. the regions of angular momentum space which are associated with fission, proton, and alpha-particle emission. If this proves to be the case, then this pattern, along with the energy spectra, can be used to calibrate the level densities in the statistical model and may develop into a useful indicator of angular momentum deposition in deep inelastic scattering of ^{86}Kr by ^{197}Au.

D. Recoil Studies of Heavy-Ion Induced Nuclear Reactions.

As an alternative approach to the studies described above, we are using recoil techniques[9-13] in the investigation of selected nuclear reactions

induced by heavy ions. The processes of particular interest in this experiment are those involving complete fusion of the beam projectile and target nucleus, followed by evaporation of nucleons or small clusters. Stacks of foils consisting of appropriately arranged targets and thin catchers are irradiated by the required heavy ion beam and the reaction products of choice are analyzed off-line (at Carnegie-Mellon University) by radioactivity identification and measurement. For the initial investigation we have selected the two reactions

$$^{60}_{28}Ni + ^{20}_{10}Ne \rightarrow ^{72}_{34}Se$$

and

$$^{40}_{20}Ca + ^{40}_{18}Ar \rightarrow ^{72}_{34}Se$$

both of which lead to the same product via rather different entrance channels. The objectives of the experiment are the determination of the energy dependences of the reaction cross-sections and the differences in excitation functions which depend on entrance channel.[14,15] Recoil range measurements will provide a test for linear momentum transfer as a criterion of complete fusion processes.

The reaction product ^{72}Se has a half-life of 8.5 d and decays exclusively by electron capture to the first excited state at 0.046 MeV in ^{72}As. Detection of the 46-keV de-excitation gamma ray provides a direct measure of the ^{72}Se formation cross-section. Although the ^{72}As ground state is radioactive with a half-life of 26 h, and hence will be in equilibrium with ^{72}Se, there is no significant interference in the spectral region of interest under the conditions we propose for counting. In a preliminary experiment carried out at the SuperHILAC accelerator of the Lawrence Berkeley Laboratory, a stack of Al foils with thin evaporated ^{60}Ni target layers was irradiated with 170-MeV ^{20}Ne ions. The stack was shipped back to Carnegie-Mellon University and the separated foils were examined to determine the ease or difficulty of evaluating

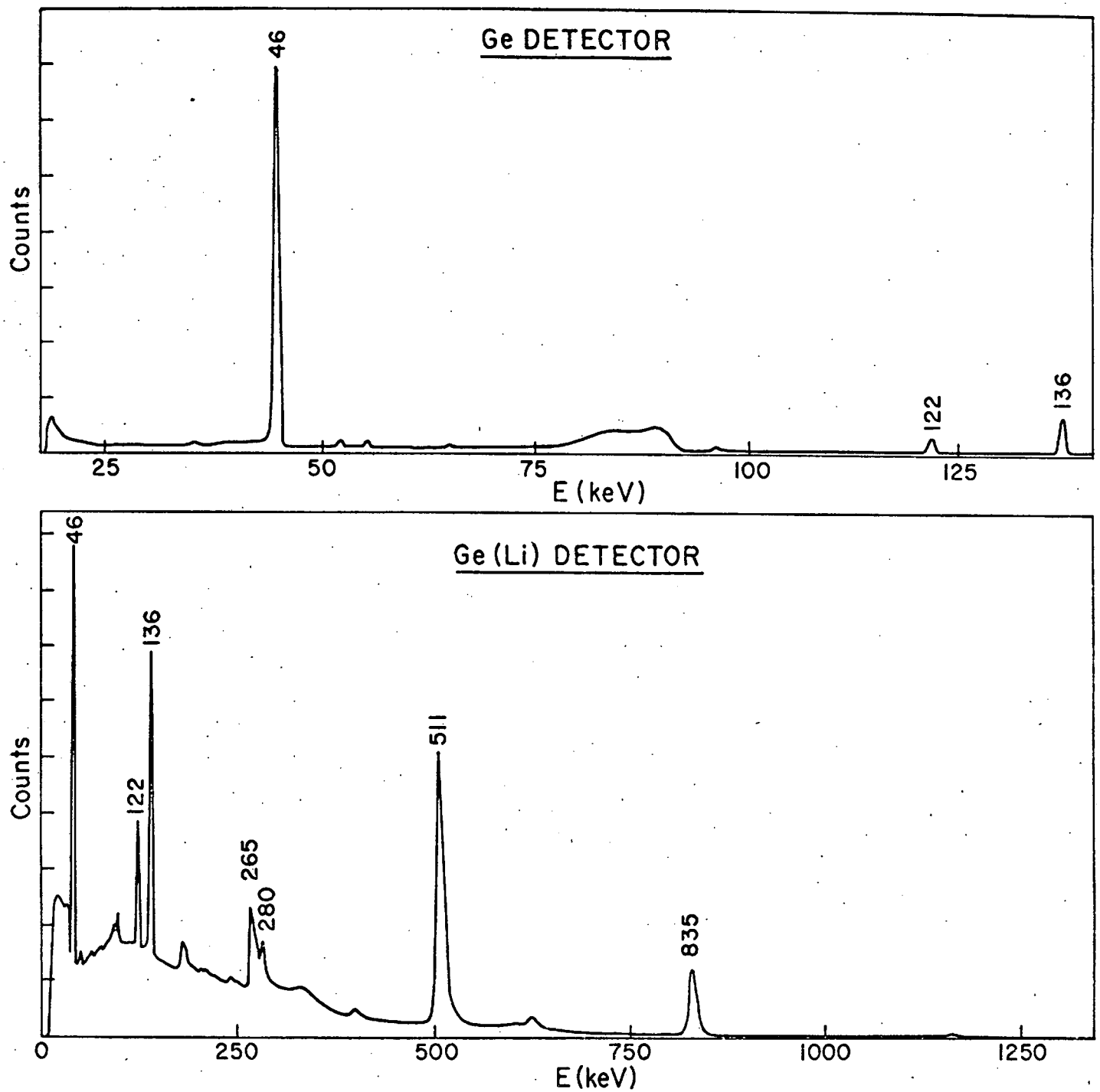
Ge DETECTOR
46
122
136
Counts
25
50
75
100
125
E (keV)
Ge (Li) DETECTOR
46
136
122
265
280
511
835
Counts
0
250
500
750
1000
1250
E (keV)

Figure 26.

the intensity under the 46-keV gamma-ray line. Some typical gamma ray spectra are shown in Fig. 26. The upper half of the figure was taken with a high resolution intrinsic Ge detector of area 200 mm^2 and thickness 5 mm, whereas the lower spectrum was recorded with a large (60 cm^3) coaxial Ge(Li) detector of conventional type. Although the latter spectrum shows the presence of activities other than ^{72}Se, it is clear from the upper spectrum in Fig. 26 that the Ge detector easily provides a very clean separation of the 46-keV gamma ray of interest and hence can serve as an assay device. The half-life measured for the 46-keV peak intensity from successive counting intervals was in excellent agreement with the expected value, $t_{1/2}$ (^{72}Se) = 8.5 d.

At the present time preparations are being made for carrying out the proposed (and approved) experiments described above.

References

1. J. R. Huizenga, J. R. Birkelund, W. U. Schröder, K. L. Wolf, and V. E. Viola, Jr., Phys. Rev. Letters 37, 885 (1976).

2. B. Gatty, D. Guerreau, M. Lefort, X. Tarrago, J. Galin, B. Cauvin, J. Girard, and H. Nifenecker, Nucl. Phys. A253, 511 (1975).

3. L. G. Moretto, J. Galin, R. Babinet, Z. Fraenkel, R. Schmitt, R. Jared, and S. G. Thompson, Nucl. Phys. A259, 173 (1976).

4. M. W. Weisfield, R. A. Williams, and A. A. Caretto, Jr., Phys. Rev. C13, 128 (1976).

5. C. D. Goodman, ORNL-TM-3946, September 1972.

6. J. R. Huizenga, Accounts of Chemical Research 9, 325 (1976). This very recent review article gives most of the relevant references.

7. R. Vandenbosch, M. P. Webb, and T. D. Thomas, Phys. Rev. C14, 143 (1976).

8. A. Fleury and J. M. Alexander, Ann. Rev. Nucl. Sci. 24, 279 (1974).

9. B. G. Harvey, Ann. Rev. Nucl. Sci. 10, 240 (1960).

10. J. M. Alexander in "Nuclear Chemistry", Vol. 1, ed. by L. Yaffe, Academic Press, New York, 1968, p. 273.

11. G. N. Simonoff and J. M. Alexander, Phys. Rev. 133, B104 (1964).

12. M. Kaplan and R. D. Fink, Phys. Rev. 134, B30 (1964).

13. M. Kaplan and V. Subrahmanyam, Phys. Rev. 153, 1186 (1967).

14. H. Gauvin, Y. Le Beyec, M. Lefort, and R. L. Hahn, Phys. Rev. C10, 722 (1974).

15. C. Cabot, H. Gauvin, Y. Le Beyec, and M. Lefort, J. Phys. Lett. 36, L-289 (1975).

Papers in Preparation

1. Angular Correlation of the 53 keV-13 keV Cascade in ^{73}Ge: Potential for High Resolution Hyperfine Interaction Studies, P. D. Johnston and M. Kaplan.

2. A Mössbauer Effect Study of Magnetic Interactions in Ferric Chloride Hexahydrate, T. X. Carroll and M. Kaplan.

3. Hyperfine Interactions of Dilute Ferric Ions in Ice: Effect of Applied Magnetic Fields, T. X. Carroll, J. C. Love, and M. Kaplan.

4. Mössbauer Resonance Investigations of Antiferromagnetic Ordering and the Spin-Flop Transition in $CoCl_2 \cdot 6H_2O$, P. D. Johnston and M. Kaplan.

5. Mössbauer Resonance Studies of Fe^{3+} Ions in HNO_3 Frozen Solutions: Effect of pH and Magnetic Fields, P. D. Johnston, M. H. Newman, and M. Kaplan

6. Perturbed Angular Correlation Studies of Chemically Generated Quadrupole Interactions in Hf Compounds, J. W. Ball and M. Kaplan.

7. Investigation of Hf Binding to Vitamin B_{12} Using Gamma Ray Perturbed Angular Correlations, J. W. Ball and M. Kaplan.

8. Quadrupole Interactions in DNA at Hf and Ag Sites Studied by Perturbed Angular Correlations, J. W. Ball and M. Kaplan.

9. Search for Enhanced ^{12}B Formation from the Reaction $^{65}Cu(^{12}C, ^{12}B)^{65}Zn$, A. A. Caretto, Jr., M. Kaplan, R. J. Spector, M. V. Yester, and R. L. Ferguson.